PREDICTION OF DAMAGE ZONE GROWTH IN COMPOSITES USING CONTINUUM DAMAGE MECHANICS

A Thesis

by

WESLEY ROSS MCLENDON

Submitted to the Office of Graduate Studies of
Texas A&M University
in partial fulfillment of the requirements for the degree of

MASTER OF SCIENCE

December 2009

Major Subject: Aerospace Engineering

PREDICTION OF DAMAGE ZONE GROWTH IN COMPOSITES USING CONTINUUM DAMAGE MECHANICS

A Thesis

by

WESLEY ROSS MCLENDON

Submitted to the Office of Graduate Studies of
Texas A&M University
in partial fulfillment of the requirements for the degree of

MASTER OF SCIENCE

Approved by:

Chair of Committee,	John D. Whitcomb
Committee Members,	Ramesh Talreja
	Xin-Lin Gao
Head of Department,	Dimitris Lagoudas

December 2009

Major Subject: Aerospace Engineering

ABSTRACT

Prediction of Damage Zone Growth in Composites
Using Continuum Damage Mechanics. (December 2009)
Wesley Ross McLendon, B.S., Texas A&M University
Chair of Advisory Committee: Dr. John D. Whitcomb

The continuum damage mechanics (CMD) approach is used to model damage zone growth in a unidirectional polymer matrix composite failing under shear stress. The long, single cracks that develop under this configuration do not match well with the homgenized distribution of defects that CDM was originally conceived to model, and so for many of the geometries and loading cases examined, the model fails to correctly predict the growth of the damage zone of the composite. From the results obtained, it is apparent that the material anisotropy of the unidirectional material tends to cause CDM to make these incorrect predictions. It is also noted that when shear failure occurs due to a local shear stress concentration near some defect which is loaded under global tensile loading, CDM yields much better predictions of damage zone growth. It is finally noted that under shear loading, certain initially damaged geometries do cause CDM to yield predictions which match the overall behavior observed experimentally. An approach is presented which attempts to create such a geometry where a new damage zone is determined to arise in order to cause CDM to correctly predict the further growth of that damage zone. Initial results are shown that suggest that this approach can improve the predictions made by CDM for the simplified geometry examined in this work.

To Dr. Kenneth Taylor at Lake Highlands High School

ACKNOWLEDGMENTS

I am grateful to those who have lent their time, knowledge, and support to aid me in the completion of this research.

I am grateful to my advisor, Dr. John Whitcomb, who has tirelessly worked to give direction to my efforts. Without his firm patience, I would likely still be sitting at a keyboard and staring at a blank screen. Without his knowledge, finite elements would be a black box that I put numbers into and got numbers out of. And without his support, I could not have afforded to attend such a fine institution to pursue graduate studies.

I am grateful to my committee members, Dr. Ramesh Talreja and Dr. Xin-Lin Gao, experts who have given of their time and knowledge to critique and guide my work.

I am grateful to the staff of the Aerospace department, particularly Dr. Walter Haisler and Mrs. Karen Knabe, who have both kindly helped me navigate the maze of forms and signatures required of graduate students.

I am grateful to my colleagues under Dr. Whitcomb - Julian Varghese, Brian Owens, Kevin Maxwell, and Deepak Goyal. They have been knowledgeable, ever-present sounding boards for my numerous questions and ideas, dedicated individuals who have worked before and beside me developing the framework on which this research was conducted, and friends who have supported me through my graduate studies.

I am grateful to Larissa Gorbatikh, whom I have not met, but to whom I an indebted for making the observations which led me to investigate the issue of modeling shear damage in composites.

I am grateful to my parents, who provided a strong foundation for me to build

my life upon.

I am grateful to my wife, who has selflessly given of herself to provide love, encouragement, and support throughout my graduate studies, all while pursuing graduate studies of her own.

I am grateful to my God, who blessed me with a mind so I might think, people in my life with which to grow and share joy, and a Savior to pay a price I could never have paid for myself.

This work was supported by the US Air Force Office of Scientific Research, funded by Contract Ref No. FA9550-07-1-0207. Any opinions, findings and conclusions or recommendations expressed in this material are those of the authors and do not necessarily reflect the views of the US Air Force Office of Scientific Research.

TABLE OF CONTENTS

CHAPTER Page

LIST OF TABLES

LIST OF FIGURES

FIGURE Page

CHAPTER I

INTRODUCTION

The use of composites in engineering has grown tremendously in the past several decades as manufacturing technology has improved and expertise in the field of design using composites has increased. As more and more products make use of composites in their design, it becomes more critical that engineers be able to predict composite behavior accurately. One aspect which is particularly challenging to model in composites is that of failure. Composites, being structures in and of themselves, are subject to a number of different failure mechanisms which operate at different scales, making them particularly difficult to model. As composite configurations become more and more complicated, as is the case for textile composites, the failure mechanisms become even more complex and exist on a wider variety of scales than typically seen in other configurations such as laminates.

One popular approach for modeling failure in composites is that of continuum damage mechanics (CDM). Failure in composites often occurs in the form of a large number of small-scale cracks, typically referred to as damage. CDM deals with damage by homogenizing it and accounting for its effect on the overall response of the material where it exists by modifying the material's contitutive properties. This method lends itself nicely to finite element analysis, where elements become the regions over which constitutive properties are altered. It is a method particularly well suited to representing distributed micro-scale cracking at a meso or macro-scale level where many analyses are performed as the geometry of the cracks is not important beyond determining how to degrade constitutive properties. For this reason, CDM

The journal model is *IEEE Journal of MicroElectroMechanical Systems*.

has been widely used to model damage in textile composite structures for which the geometry of the architecture can become very complicated.

The CDM approach for modeling mechanical damage in composites is typically broken down into two major components. The first is the failure criteria. This involves determining where in a model failure has occurred as well as the nature of the damage which now exists as a result of that failure. Types of failure possible in composites include matrix cracking, fiber breakage, and fiber buckling, among others. The type of damage which occurs is generally determined by the stress component which causes the failure. The second major aspect of CDM involves the modification of material properties due to damage. Based on the damage which is predicted to have occurred by the failure criterion, the material properties are altered in a manner so that the homogenized effect of the damage is captured by the new constitutive properties.

It has recently been observed by Gorbatikh, et al. [1] that CDM fails to properly predict damage propagation in textile composites which fail due to shear stress acting along the fibers. It was observed from analyses that in 45° braid tows in a textile composite under tension (a situation leading to high shear loading of the braid tows), CDM predicted a damage zone that was unrealistically large and which developed in a direction contrary to the expected behavior of damage growth along the fibers (Figure 1). Two configurations were compared to investigate this phenomena. The first was a discrete crack running along the fiber direction. The second configuration was a circular region with a diameter equal to the length of the crack with material properties degraded according to the Murakami-Ohno degradation scheme [2],[3] for a composite with failure due to transverse or shear loading (Figure 2), which was analyzed using the elasticity solution by Eshelby [4]. When these two configurations were placed under shear loading, the stress concentrations leading to damage growth occurred at different locations, suggesting that the two models would predict different

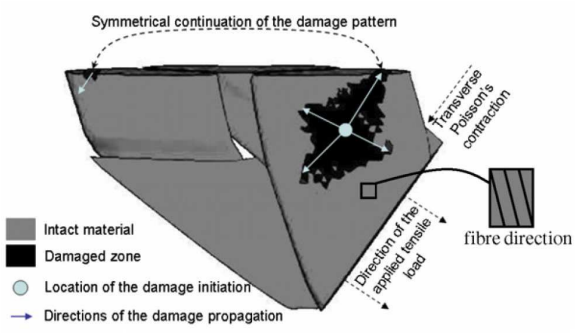

Fig. 1. Damage growth prediction observed by Gorbatich et al. [1]

damage growth behaviors. The Murikami-Ohno model was modified in an attempt to account for differences between the configurations, but the modified model still failed to predict a maximum stress concentration location matching that of a discrete crack. It was finally concluded that CDM is unable to correctly predict damage growth resulting from shear failure in textiles because the damage which occurs under shear stress in such models (tow-scale cracking along the fiber direction) is discrete and exists on a large scale, characteristics which do not correspond to the distributed small-scale defects that CDM was originally conceived to model.

A. Literature Survey

The continuum damage mechanics approach was originally proposed by Kachanov in 1958 [5] as a means of modeling creep. Talreja [6] extended CDM to composite

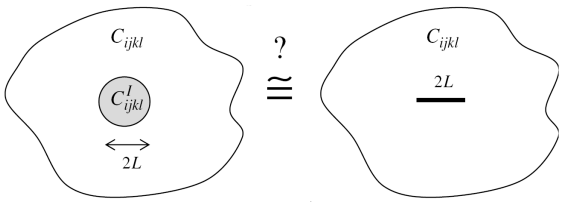

Fig. 2. Configurations compared by Gorbatich et al. [1]

materials using a vector-field to describe the damage. Within textile composites, CDM has been extensively used as a tool for predicting the macro-scale response of a textile architecture based upon meso or tow scale analyses of unit cells. Among the most popular models used for such analyses are those developed by Blackketter et al. [7] and Murakami and Ohno [2, 3]. Chapman and Whitcomb [8] developed a model which, while similar to that of Blackketter, differed slightly with regards to some of the factors used to degrade material properties of damaged material. Zako et al. [9] developed a model which utilizes a tensor to describe the damage of the material, thereby affecting off-diagonal terms of the compliance and stiffness matrices, for the analysis of failure in unidirectional composites. In later years this model was adapted and utilized in conjunction with the Murikami Ohno model in an analysis which tracked damage evolution in plain-weave composites loaded under tension [10]. Another model, proposed by Chioy and Tamma [11], makes use of physical arguments to determine how properties should be degraded for various failure modes. In the work performed by Gorbatikh et al., it was noted that previous work in progressive damage analysis of textiles has not generally included a critical inspection of damage propagation in tows undergoing shear stress. They worked to develop an improved degradation model based on Murikami-Ohno by matching the elastic response of a degraded region to that of a crack. It was observed that the Murikami-Ohno model in its basic form over-estimated how much the stiffness, particularly the shear stiffness, should be degraded for the region. However, as mentioned, this effort did not allow accurate prediction of the direction of damage propagation for shear extending from the initially degraded region.

B. Overview of Research

The research reported by Gorbatikh et al. [1] did not include an investigation of the shape of the initially damaged region. The shape of an inclusion greatly affects the stress distribution around it, as is evidenced by the differences in stress around a sharp crack and a hole under the same loading. For this research, it was hypothesized that sufficient directionality in an initially damaged region may allow a CDM approach to correctly predict the further growth of damage resulting from shear stress. Therefore, an investigation was conducted into a number of simple configurations spanning various geometries which result in damage occurring due to shear. Models under global shear loads, as well as models experiencing local shear concentrations resulting from defects such as holes under tensile loading were examined. Also, models which are representative of a finite element mesh experiencing damage initiation (with just a few elements damaged) were investigated.

Based on observations made from these investigations, a possible modification to the CDM approach was developed which aims to include geometric information about the damage which is not contained within the basic CDM algorithm. This modification was applied to a very simple configuration. The work presented is intended to put forward a possible improvement to the CDM algorithm for cases in which discrete damage may grow to a scale too large to be considered part of a continuum, such as the case observed by Gorbatikh et al. [1]; it is not intended as a rigorous validation of the modification.

CHAPTER II

FORMULATION OF ELASTIC FINITE ELEMENTS IN THREE DIMENSIONS

The analyses performed in this work used an implementation of the three-dimensional elastic finite element method. Although the configurations and loadings of the analyses in this work were primarily two dimensional in nature, the particular routines associated with damage modeling which were used were implemented in three dimensions, and so three dimensional elements were used.

The finite element method consists of the discretization of the physical problem domain into a mesh. Various constitutive properties are then assigned to sub domains within the mesh, generally corresponding to various materials. These constitutive properties lead to the definition of element stiffnesses which are determined from the governing equations of equilibrium. Boundary conditions defining either force or displacement are defined for all surfaces of the mesh. The definition of sufficient boundary conditions leads to the formation of a system of linear equations whose solution is the set of nodal displacements and forces resulting in static equilibrium for the entire problem domain. These displacements can be spatially differentiated to obtain strains through kinematic relationships, which can then be converted into stresses using constitutive relationships. The mathematical details of the finite element method are discussed in detail in the following sections.

A. Kinematic Relationships

The constitutive relationship between strain and stress in a body depends first on how strain is defined for the body. Assume a body is initially in some reference configuration. Two refernce frames exist for describing the configuration of the body. The first, the Lagrangian frame, defines the configuration of the body using reference, or

material coordiates $X_i(t)$. The second, Eulerian reference frame, defines the configuration of a deformed body by the spatial coordinates $x_i(t)$ which follow the body as it deforms. The Eulerian description of the body's configuration can be expressed in terms of the Lagrangian reference frame by a mapping function $\chi(X_i, t)$ such that $x_i = \chi(X_i, t)$. The deformation gradient is then defined as

$$F_{ij} = \frac{\partial x_i}{\partial X_j} = \frac{\partial \chi(X_i, t)}{\partial X_j} \tag{2.1}$$

Also define the displacement of some point on the body as

$$u_i = x_i - X_i \tag{2.2}$$

Next, define B_{ij} and C_{ij} the left and right stretch tensors, respectively.

$$\begin{aligned} B_{ij} &= F_{ik}F_{jk} \\ C_{ij} &= F_{ki}F_{kj} \end{aligned} \tag{2.3}$$

From these stretch tensors, one can derive two strains. First, the Green - St. Venant Strain is defined as

$$\begin{aligned} E_{ij} &= \frac{1}{2}\left(C_{ij} - \delta_{ij}\right) \\ &= \frac{1}{2}\left(F_{ki}F_{kj} - \delta_{ij}\right) \\ &= \frac{1}{2}\left(\frac{\partial u_j}{\partial X_i} + \frac{\partial u_i}{\partial X_j} + \frac{\partial u_k}{\partial X_i}\frac{\partial u_k}{\partial X_j}\right) \end{aligned} \tag{2.4}$$

where δ_{ij} is the Kronecker delta. Second, the Almansi-Hamel Strain is defined as

$$\begin{aligned} e_{ij} &= \frac{1}{2}\left(\delta_{ij} - B_{ij}^{-1}\right) \\ &= \frac{1}{2}\left(\delta_{ij} - \left(F_{ik}F_{jk}\right)^{-1}\right) \\ &= \left(\frac{\partial u_j}{\partial x_i} + \frac{\partial u_i}{\partial x_j} - \frac{\partial u_k}{\partial x_i}\frac{\partial u_k}{\partial x_j}\right) \end{aligned} \tag{2.5}$$

Now, the linearizing assumption will be inserted into the derivation. It will be assumed for all deformations, that the deformation gradient is small. That is

$$\|\tfrac{\partial u_i}{\partial X_i}\| = \mathbf{O}(\delta) \quad \delta \ll 1 \tag{2.6}$$

It follows that

$$\frac{\partial u_i}{\partial X_i} = \frac{\partial u_i}{\partial x_i} + \mathbf{O}(\delta^2) \tag{2.7}$$

Appealing to the assertions in Eq. (2.6) and Eq. (2.7) in the context of the strains of Eq. (2.4) and Eq. (2.5) yields

$$\begin{aligned} E_{ij} &= \varepsilon_{ij} + \mathbf{O}(\delta^2) \\ e_{ij} &= \varepsilon_{ij} + \mathbf{O}(\delta^2) \end{aligned} \tag{2.8}$$

where ε_{ij} is the linearized strain tensor, defined as

$$\begin{aligned} \varepsilon_{ij} &= \frac{1}{2}\left(\frac{\partial u_j}{\partial X_i} + \frac{\partial u_i}{\partial X_j}\right) \\ &\approx \frac{1}{2}\left(\frac{\partial u_j}{\partial x_i} + \frac{\partial u_i}{\partial x_j}\right) \end{aligned} \tag{2.9}$$

It can be seen that the strain tensor will always be symmetric, as the addition of a matrix with its transpose always results in a symmetric matrix. Also, it can be seen that the linearized strain is very nearly equal when taken in either a Eulerian or Lagrangian reference frame. From this point forward in the derivations, the distinction between the two becomes unimportant, and all spatial coordinates will be given in the form x_i.

B. Constitutive Relationships

With the linearized strain now defined, it is possible to clearly state the constitutive relationship between stress and strain. The linear elastic constitutive model is founded

on two major assumptions. The first is that for a given material, the relationship between stress and strain is linear within the loads experienced by the model. In a sense, this is not true of the analyses performed in this work as once a load results in failure, the constitutive properties of the material will be changed. Once the properties are reduced, the material is once again treated as a linear elastic material until some other failure mode occurs, so in reality any given portion of the analysis is linear elastic. The second assumption of linear elastic constitutive relationships is that the body will not dissipate energy and will return to its reference configuration upon removal of the load (in essence, it will exhibit a coefficient of restitution equaling 1). Within a given analysis step of the work performed here, this holds true, although from step to step energy is released as material stiffness is degraded at locations of failure.

The most general relationship between the stress and strain tensors is given by

$$\sigma_{ij} = C_{ijkl}\varepsilon_{kl} \tag{2.10}$$

where C_{ijkl} is a fourth-order tensor, often referred to as the stiffness tensor, containing 81 constants. It is convenient to represent this fourth order tensor as a two-dimensional matrix by expressing the stress and strain tensors as vectors with 6 components by exploiting their symmetry. Like the strain tensor, the stress tensor for a static body is symmetric. The symmetry of the stress tensor is required to maintain equilibrium for angular momentum for all points in the body. Exploiting these symmetries implies that $C_{ijkl} = C_{jikl} = C_{ijlk}$ and reduces the number of constants

relating stress and strain from 81 to 36 as can be seen in the following relationship.

$$\begin{pmatrix} \sigma_{11} \\ \sigma_{22} \\ \sigma_{33} \\ \sigma_{23} \\ \sigma_{31} \\ \sigma_{12} \end{pmatrix} = \begin{pmatrix} C_{1111} & C_{1122} & C_{1133} & C_{1123} & C_{1131} & C_{1112} \\ C_{2211} & C_{2222} & C_{2233} & C_{2223} & C_{2231} & C_{2212} \\ C_{3311} & C_{3322} & C_{3333} & C_{3323} & C_{3331} & C_{3312} \\ C_{2311} & C_{2322} & C_{2333} & C_{2323} & C_{2331} & C_{2312} \\ C_{3111} & C_{3122} & C_{3133} & C_{3123} & C_{3131} & C_{3112} \\ C_{1211} & C_{1222} & C_{1233} & C_{1223} & C_{1231} & C_{1212} \end{pmatrix} \begin{pmatrix} \varepsilon_{11} \\ \varepsilon_{22} \\ \varepsilon_{33} \\ 2\varepsilon_{23} \\ 2\varepsilon_{31} \\ 2\varepsilon_{12} \end{pmatrix} \tag{2.11}$$

The overall symmetry of the stiffness tensor is established by relating stress and strain using the strain energy density functional U. This relationship is given as

$$\sigma_{ij} = \frac{\partial U}{\partial \varepsilon_{ij}} = C_{ijkl}\varepsilon_{kl} \quad \Longrightarrow \quad \frac{\partial^2 U}{\partial \varepsilon_{ij}\partial \varepsilon_{kl}} = C_{ijkl} \tag{2.12}$$

which implies that $C_{ijkl} = C_{klij}$ due to the fact that the order of differentiation will not change its result. This reduces the total number of independent constants relating stress and strain to 21.

The number of terms in $\boldsymbol{C}$ can be further reduced by appealing to material symmetries. For the analyses in this work, it will be assumed that all materials are orthotropic. That is, all materials possess three planes of symmetry about which a reflection can take place with no change in the response of the material. It is assumed that the material will be defined such that these planes of symmetry are aligned with the coordinate axes. The orthogonal transformation matrices associated with these reflections are given in table I.

Table I. Orthogonal reflection transformation matrices

Reflection Plane	Transformation Tensor
23	$\boldsymbol{Q} = \begin{pmatrix} -1 & 0 & 0 \\ 0 & 1 & 0 \\ 0 & 0 & 1 \end{pmatrix}$
31	$\boldsymbol{Q} = \begin{pmatrix} 1 & 0 & 0 \\ 0 & -1 & 0 \\ 0 & 0 & 1 \end{pmatrix}$
12	$\boldsymbol{Q} = \begin{pmatrix} 1 & 0 & 0 \\ 0 & 1 & 0 \\ 0 & 0 & -1 \end{pmatrix}$

The stiffness matrix resulting from such a reflection is given as

$$C'_{ijkl} = Q_{ip}Q_{jq}Q_{kr}Q_{ls}C_{pqrs} \tag{2.13}$$

Provided that Q_{ij} represents a reflection about a material plane of symmetry, it can be stated that

$$C_{ijkl} = C'_{ijkl} \tag{2.14}$$

Applying Eq. (2.13) and Eq. (2.14) to Eq. (2.11), it is found that a number of terms must equal zero to satisfy the material symmetry. The resulting stiffness tensor for orthotropic materials contains 9 constants as follows.

$$\boldsymbol{C} = \begin{pmatrix} C_{1111} & C_{1122} & C_{1133} & 0 & 0 & 0 \\ C_{1122} & C_{2222} & C_{2233} & 0 & 0 & 0 \\ C_{1133} & C_{2233} & C_{3333} & 0 & 0 & 0 \\ 0 & 0 & 0 & C_{2323} & 0 & 0 \\ 0 & 0 & 0 & 0 & C_{3131} & 0 \\ 0 & 0 & 0 & 0 & 0 & C_{1212} \end{pmatrix} \tag{2.15}$$

Material properties are given in terms of engineering constants. These constants are most conveniently expressed in the compliance tensor $\boldsymbol{S}$, which is the inverse of the

stiffness tensor. The compliance tensor for orthotropic materials relates strain to stress in the following manner.

$$\begin{pmatrix} \varepsilon_{11} \\ \varepsilon_{22} \\ \varepsilon_{33} \\ 2\varepsilon_{23} \\ 2\varepsilon_{31} \\ 2\varepsilon_{12} \end{pmatrix} = \begin{pmatrix} \frac{1}{E_1} & -\frac{\nu_{12}}{E_1} & -\frac{\nu_{13}}{E_1} & 0 & 0 & 0 \\ -\frac{\nu_{21}}{E_2} & \frac{1}{E_2} & -\frac{\nu_{23}}{E_2} & 0 & 0 & 0 \\ -\frac{\nu_{31}}{E_3} & -\frac{\nu_{32}}{E_3} & \frac{1}{E_3} & 0 & 0 & 0 \\ 0 & 0 & 0 & \frac{1}{G_{23}} & 0 & 0 \\ 0 & 0 & 0 & 0 & \frac{1}{G_{31}} & 0 \\ 0 & 0 & 0 & 0 & 0 & \frac{1}{G_{12}} \end{pmatrix} \begin{pmatrix} \sigma_{11} \\ \sigma_{22} \\ \sigma_{33} \\ \sigma_{23} \\ \sigma_{31} \\ \sigma_{12} \end{pmatrix} \tag{2.16}$$

$$\frac{\nu_{23}}{E_2} = \frac{\nu_{32}}{E_3} \qquad \frac{\nu_{31}}{E_3} = \frac{\nu_{13}}{E_1} \qquad \frac{\nu_{12}}{E_1} = \frac{\nu_{21}}{E_2}$$

C. Governing Equations of Elasticity and the Weak Form

The primary equation governing the loading of elastic bodies is that of equilibrium. For static bodies, the equilibrium equation takes the following form:

$$\frac{\partial \sigma_{ij}}{\partial x_j} + \rho b_i = 0 \tag{2.17}$$

where ρ is density and b_i is the specific body force. Eq. (2.17) is then multiplied by test functions (often referred to as virtual displacements) δu_i and integrated over the problem domain Ω. The resulting "weak form" of the equation of equilibrium is

$$\int_\Omega \delta u_i \left(\frac{\partial \sigma_{ij}}{\partial x_j} + \rho b_i \right) d\Omega = \int_\Omega \left(\delta u_i \frac{\partial \sigma_{ij}}{\partial x_j} + \delta u_i \rho b_i \right) d\Omega = 0 \tag{2.18}$$

The first term of Eq. (2.18) can be expanded through integration by parts.

$$\int_\Omega \left(\delta u_i \frac{\partial \sigma_{ij}}{\partial x_j} \right) d\Omega = \int_\Omega \frac{\partial \left(\delta u_i \sigma_{ij} \right)}{\partial x_j} d\Omega - \int_\Omega \left(\frac{\partial \delta u_i}{\partial x_j} \sigma_{ij} \right) d\Omega \tag{2.19}$$

Applying the result of Eq. (2.19) into Eq. (2.18) yields the following expression for the weak form.

$$\int_{\Omega} \frac{\partial \left(\delta u_i \sigma_{ij}\right)}{\partial x_j} d\Omega + \int_{\Omega} \left(\rho b_i \delta u_i - \frac{\partial \delta u_i}{\partial x_j} \sigma_{ij} \right) d\Omega = 0 \tag{2.20}$$

Applying Gauss's divergence theorem to the first term in Eq. (2.20) yields

$$\int_{\Gamma} \left(\delta u_i \sigma_{ij} n_j\right) d\Gamma + \int_{\Omega} \left(\rho b_i \delta u_i - \frac{\partial \delta u_i}{\partial x_j} \sigma_{ij} \right) d\Omega = 0 \tag{2.21}$$

Γ is the surface of the domain Ω, and n_i is the normal vector at a point on Γ. Now, Cauchy's stress formula for the traction on a surface, T_i, will be incorporated.

$$T_i = \sigma_{ij} n_j \tag{2.22}$$

Incorporating Eq. (2.22) into Eq. (2.21) yields

$$\int_{\Gamma} \left(\delta u_i T_i\right) d\Gamma + \int_{\Omega} \left(\rho b_i \delta u_i - \frac{\partial \delta u_i}{\partial x_j} \sigma_{ij} \right) d\Omega = 0 \tag{2.23}$$

Additionally, The symmetry of the Cauchy stress tensor and Eq. (2.9) allow the following equivalence to be established

$$\frac{\partial \delta u_i}{\partial x_j} \sigma_{ij} = \delta \epsilon_{ij} \sigma_{ij} \tag{2.24}$$

Applying the relationship established in Eq. (2.24) to the last term in the volume integral of Eq. (2.23) yields the following

$$\int_{\Gamma} \left(\delta u_i T_i\right) d\Gamma + \int_{\Omega} \left(\rho b_i \delta u_i - \delta \varepsilon_{ij} \sigma_{ij} \right) d\Omega = 0 \tag{2.25}$$

Now Galerkin approximations will be used to represent the trial function δu_i. The approximation is based upon the principle that a function can be represented as an infinite sum of smooth basis functions $\psi^{(m)}$. In the finite element analysis, there will be as many basis functions as there are nodes in the element. This results in the

trial function taking the following form.

$$\delta u_i = \sum_{m=1}^{n} \delta u_i^{(m)} \psi^{(m)} \tag{2.26}$$

such that m denotes the m^{th} node in the element and n is the total number of nodes in the element. All components of all nodal displacements $u_i^{(m)}$ for an element will be combined into one vector q_α for convenience (in essence, a vector of all degrees of freedom for the element).

$$q_\alpha = \left(u_1^{(1)}, u_2^{(1)}, u_3^{(1)} \cdots, u_1^{(m)}, u_2^{(m)}, u_3^{(m)}, \cdots, u_1^{(n)}, u_2^{(n)}, u_3^{(n)} \right) \tag{2.27}$$

such that subscripts represent the component of displacement and superscripts represent the node of the element. Virtual displacement and strain can now be expressed in the following manner.

$$\delta u_i = \frac{\partial u_i}{\partial q_\alpha} \delta q_\alpha \tag{2.28}$$

$$\delta \varepsilon_{ij} = \frac{\partial \varepsilon_{ij}}{\partial q_\alpha} \delta q_\alpha \tag{2.29}$$

Substitution of Eq. (2.28) and Eq. (2.29) into Eq. (2.25) and summing over the nodes of an element yields

$$\delta q_\alpha \left(\int_\Gamma \left(\frac{\partial u_i}{\partial q_\alpha} T_i \right) d\Gamma + \int_\Omega \left(\rho b_i \frac{\partial u_i}{\partial q_\alpha} \right) d\Omega - \int_\Omega \left(\frac{\partial \varepsilon_{ij}}{\partial q_\alpha} \sigma_{ij} \right) d\Omega \right) = 0 \tag{2.30}$$

Since this relationship must hold for any arbitrary non-zero value of the test function δq_α, it is necessary that for all values of α

$$\int_\Gamma \left(\frac{\partial u_i}{\partial q_\alpha} T_i \right) d\Gamma + \int_\Omega \left(\rho b_i \frac{\partial u_i}{\partial q_\alpha} \right) d\Omega - \int_\Omega \left(\frac{\partial \varepsilon_{ij}}{\partial q_\alpha} \sigma_{ij} \right) d\Omega = 0 \tag{2.31}$$

For convenience, Voigt notation will be used from this point forward to represent the

strain and stress tensors as follows

$$\boldsymbol{\varepsilon} = \varepsilon_{ij} = \begin{pmatrix} \varepsilon_{11} & \varepsilon_{12} & \varepsilon_{13} \\ \varepsilon_{21} & \varepsilon_{22} & \varepsilon_{23} \\ \varepsilon_{31} & \varepsilon_{32} & \varepsilon_{33} \end{pmatrix} = \begin{pmatrix} \varepsilon_{11} \\ \varepsilon_{22} \\ \varepsilon_{33} \\ \varepsilon_{23} = \varepsilon_{32} \\ \varepsilon_{31} = \varepsilon_{13} \\ \varepsilon_{12} = \varepsilon_{21} \end{pmatrix} = \varepsilon_k = \begin{pmatrix} \varepsilon_1 \\ \varepsilon_2 \\ \varepsilon_3 \\ \varepsilon_4 \\ \varepsilon_5 \\ \varepsilon_6 \end{pmatrix} \tag{2.32}$$

This notation simplifies the formation of the strain-displacement matrix, $B_{k\alpha}$, which is defined through the kinematic relationship defining strain in Eq. (2.9) in conjunction with the Galerkin approximation for displacement of Eq. (2.26).

$$B_{k\alpha} = \frac{\partial \varepsilon_k}{\partial q_\alpha} = \left(\begin{array}{ccc|c|ccc} \frac{\partial \psi^{(1)}}{\partial x_1} & 0 & 0 & & \frac{\partial \psi^{(n)}}{\partial x_1} & 0 & 0 \\ 0 & \frac{\partial \psi^{(1)}}{\partial x_2} & 0 & & 0 & \frac{\partial \psi^{(n)}}{\partial x_2} & 0 \\ 0 & 0 & \frac{\partial \psi^{(1)}}{\partial x_3} & \cdots & 0 & 0 & \frac{\partial \psi^{(n)}}{\partial x_3} \\ 0 & \frac{\partial \psi^{(1)}}{\partial x_2} & \frac{\partial \psi^{(1)}}{\partial x_3} & & 0 & \frac{\partial \psi^{(n)}}{\partial x_2} & \frac{\partial \psi^{(n)}}{\partial x_3} \\ \frac{\partial \psi^{(1)}}{\partial x_1} & 0 & \frac{\partial \psi^{(1)}}{\partial x_3} & & \frac{\partial \psi^{(n)}}{\partial x_1} & 0 & \frac{\partial \psi^{(n)}}{\partial x_3} \\ \frac{\partial \psi^{(1)}}{\partial x_1} & \frac{\partial \psi^{(1)}}{\partial x_2} & 0 & & \frac{\partial \psi^{(n)}}{\partial x_1} & \frac{\partial \psi^{(n)}}{\partial x_2} & 0 \end{array}\right) \tag{2.33}$$

The strain displacement matrix is used to calculate strains based on the element displacement vector by

$$\varepsilon_k = B_{k\alpha} q_\alpha \tag{2.34}$$

This results in the final term of Eq. (2.31) taking the form

$$\int_\Omega \left(B_{k\alpha} \sigma_k\right) d\Omega \tag{2.35}$$

Furthermore, through the constitutive relationship of Eq. (2.10) the stress tensor can

be represented in the following manner

$$\sigma_k = C_{kl}\varepsilon_l = C_{kl}B_{l\alpha}q_\alpha \tag{2.36}$$

Incorporating Eq. (2.36) into Eq. (2.35) leads to the formation of the familiar element stiffness matrix in the following manner

$$\int_{\Omega_e} (B_{k\alpha}\sigma_k)\, d\Omega_e = \int_{\Omega_e} (B_{k\alpha}C_{kl}B_{l\beta}q_\beta)\, d\Omega_e = \int_{\Omega_e} (B_{k\alpha}C_{kl}B_{l\beta})\, d\Omega_e\, q_\beta = K_{\alpha\beta}q_\beta \tag{2.37}$$

or, in matrix form (with boldface representing a matrix or vector),

$$\int_{\Omega_e} \left(\boldsymbol{B}^{\mathrm{T}}\boldsymbol{\sigma}\right) d\Omega_e = \int_{\Omega_e} \left(\boldsymbol{B}^{\mathrm{T}}\boldsymbol{C}\boldsymbol{B}\mathbf{q}\right) d\Omega_e = \int_{\Omega_e} \left(\boldsymbol{B}^{\mathrm{T}}\boldsymbol{C}\boldsymbol{B}\right) d\Omega_e\, \mathbf{q} = \boldsymbol{K}\mathbf{q} \tag{2.38}$$

The subscript e signifies that the integral is taken over the domain of a single element. The partial derivative of the displacement field with respect to the nodal displacements which appears in the remaining terms of Eq. (2.31) can be expressed using a method similar to Eq. (2.33).

$$\frac{\partial u_i}{\partial q_\alpha} = \left(\begin{array}{ccc|c|ccc|c|ccc} \psi^{(1)} & 0 & 0 & & \psi^{(m)} & 0 & 0 & & \psi^{(n)} & 0 & 0 \\ 0 & \psi^{(1)} & 0 & \cdots & 0 & \psi^{(m)} & 0 & \cdots & 0 & \psi^{(n)} & 0 \\ 0 & 0 & \psi^{(1)} & & 0 & 0 & \psi^{(m)} & & 0 & 0 & \psi^{(n)} \end{array}\right) \tag{2.39}$$

This leads to the creation of the element force vector as follows

$$
\begin{aligned}
f_\alpha &= \int_{\Gamma_e} \left(T_i \frac{\partial u_i}{\partial q_\alpha} \right) d\Gamma_e + \int_{\Omega_e} \left(\rho b_i \frac{\partial u_i}{\partial q_\alpha} \right) d\Omega_e \\
&= \begin{pmatrix}
\int_{\Gamma_e} \left(T_1 \psi^{(1)} \right) d\Gamma_e + \int_{\Omega_e} \left(\rho b_1 \psi^{(1)} \right) d\Omega_e \\
\int_{\Gamma_e} \left(T_2 \psi^{(1)} \right) d\Gamma_e + \int_{\Omega_e} \left(\rho b_2 \psi^{(1)} \right) d\Omega_e \\
\int_{\Gamma_e} \left(T_3 \psi^{(1)} \right) d\Gamma_e + \int_{\Omega_e} \left(\rho b_3 \psi^{(1)} \right) d\Omega_e \\
\vdots \\
\int_{\Gamma_e} \left(T_1 \psi^{(m)} \right) d\Gamma_e + \int_{\Omega_e} \left(\rho b_1 \psi^{(m)} \right) d\Omega_e \\
\int_{\Gamma_e} \left(T_2 \psi^{(m)} \right) d\Gamma_e + \int_{\Omega_e} \left(\rho b_2 \psi^{(m)} \right) d\Omega_e \\
\int_{\Gamma_e} \left(T_3 \psi^{(m)} \right) d\Gamma_e + \int_{\Omega_e} \left(\rho b_3 \psi^{(m)} \right) d\Omega_e \\
\vdots \\
\int_{\Gamma_e} \left(T_1 \psi^{(n)} \right) d\Gamma_e + \int_{\Omega_e} \left(\rho b_1 \psi^{(n)} \right) d\Omega_e \\
\int_{\Gamma_e} \left(T_2 \psi^{(n)} \right) d\Gamma_e + \int_{\Omega_e} \left(\rho b_2 \psi^{(n)} \right) d\Omega_e \\
\int_{\Gamma_e} \left(T_3 \psi^{(n)} \right) d\Gamma_e + \int_{\Omega_e} \left(\rho b_3 \psi^{(n)} \right) d\Omega_e
\end{pmatrix}
\end{aligned}
\tag{2.40}
$$

Eq. (2.37) and Eq. (2.40) allow the weak formulation of Eq. (2.31) to be expressed for an element in the familiar form of a linear system of equations

$$
\boldsymbol{K}\mathbf{q} = \mathbf{f} \tag{2.41}
$$

D. Element Formulations

1. Basis Functions

Recall from Eq. (2.26) that the displacement throughout an element is determined by summing the products of the nodal displacements and their corresponding basis functions. The formation of basis functions for an element is critical to its computation. Generally, a basis function for a node is formed such that it possesses a value of unity at that node and a value of zero at all other nodes. For these elements, the

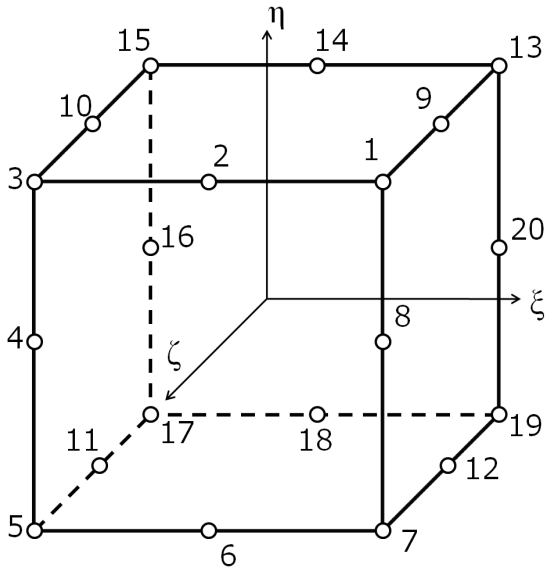

Fig. 3. 20 node hexahedron master element

basis functions will be in the form of polynomials. This will allow their exact integration using quadrature rules, the importance of which will be explained in following subsections.

Although elements can assume non-regular shapes in the problem domain described in the global coordinates (x, y, z), the shape function formulations will be calculated in the master element coordinate system defined by (ξ, η, ζ), in which the element assumes a regular shape and extends from -1 to 1 in all coordinate directions. For these analyses, 20 node hexahedron elements are used. The node numbering convention for such an element takes the form seen in figure 3.

The 20 node hexahedron is often referred to as a type of serendipity element because it is a quadratic element in which all the nodes exist on edges (as opposed to the Lagrange family of elements which possess internal nodes). It is a quadratic element because as will be seen, the basis functions are second-order polynomials. The process for forming the basis functions occurs in the following manner. For the first node, which possesses coordinates $(1, 1, 1)$, it is desired to construct a basis function with a value of unity at node 1 and a value of zero at all other nodes. Therefore, the basis function for node 1 should vanish on the planes defined by the following functions.

$$\begin{aligned} \xi + 1 &= 0 \qquad \text{(nodes 3, 4, 5, 10, 11, 15, 16, and 17)} \\ \eta + 1 &= 0 \qquad \text{(nodes 5, 6, 7, 11, 12, 17, 18, and 19)} \\ \zeta + 1 &= 0 \qquad \text{(nodes 13, 14, 15, 16, 17, 18, 19, and 20)} \\ \xi + \eta + \zeta - 2 &= 0 \qquad \text{(nodes 2, 8, and 9)} \end{aligned} \tag{2.42}$$

This yields a function of the following form

$$\psi^{(1)}(\xi, \eta, \zeta) = C(\xi + 1)(\eta + 1)(\zeta + 1)(\xi + \eta + \zeta - 2) \tag{2.43}$$

It is desired that $\psi^{(1)}$ have a value of unity at node 1, resulting in

$$\psi^{(1)}(\xi, \eta, \zeta) = \frac{1}{8}(\xi + 1)(\eta + 1)(\zeta + 1)(\xi + \eta + \zeta - 2) \tag{2.44}$$

This convention can be followed for the remainder of the nodes, yielding the following

set of basis functions for the master element.

$$
\begin{aligned}
\psi^{(1)} &= \tfrac{1}{8}(\xi+1)(\eta+1)(\zeta+1)(\xi+\eta+\zeta-2)\\
\psi^{(2)} &= -\tfrac{1}{4}(\xi^2-1)(\eta+1)(\zeta+1)\\
\psi^{(3)} &= \tfrac{1}{8}(\xi-1)(\eta+1)(\zeta+1)(\xi-\eta-\zeta+2)\\
\psi^{(4)} &= \tfrac{1}{4}(\xi-1)(\eta^2-1)(\zeta+1)\\
\psi^{(5)} &= \tfrac{1}{8}(\xi-1)(\eta-1)(\zeta+1)(-\xi-\eta+\zeta-2)\\
\psi^{(6)} &= \tfrac{1}{4}(\xi^2-1)(\eta-1)(\zeta+1)\\
\psi^{(7)} &= \tfrac{1}{8}(\xi+1)(\eta-1)(\zeta+1)(-\xi+\eta-\zeta+2)\\
\psi^{(8)} &= -\tfrac{1}{4}(\xi+1)(\eta^2-1)(\zeta+1)\\
\psi^{(9)} &= -\tfrac{1}{4}(\xi+1)(\eta+1)(\zeta^2-1)\\
\psi^{(10)} &= \tfrac{1}{4}(\xi-1)(\eta+1)(\zeta^2-1)\\
\psi^{(11)} &= -\tfrac{1}{4}(\xi-1)(\eta-1)(\zeta^2-1)\\
\psi^{(12)} &= \tfrac{1}{4}(\xi+1)(\eta-1)(\zeta^2-1)\\
\psi^{(13)} &= \tfrac{1}{8}(\xi+1)(\eta+1)(\zeta-1)(-\xi-\eta+\zeta+2)\\
\psi^{(14)} &= \tfrac{1}{4}(\xi^2-1)(\eta+1)(\zeta-1)\\
\psi^{(15)} &= \tfrac{1}{8}(\xi-1)(\eta+1)(\zeta-1)(-\xi+\eta-\zeta-2)\\
\psi^{(16)} &= -\tfrac{1}{4}(\xi-1)(\eta^2-1)(\zeta-1)\\
\psi^{(17)} &= \tfrac{1}{8}(\xi-1)(\eta-1)(\zeta-1)(\xi+\eta+\zeta+2)\\
\psi^{(18)} &= -\tfrac{1}{4}(\xi^2-1)(\eta-1)(\zeta-1)\\
\psi^{(19)} &= \tfrac{1}{8}(\xi+1)(\eta-1)(\zeta-1)(\xi-\eta-\zeta-2)\\
\psi^{(20)} &= \tfrac{1}{4}(\xi+1)(\eta^2-1)(\zeta-1)
\end{aligned}
\tag{2.45}
$$

2. Spatial Mapping

The integrations of Eq. (2.37) are performed using Gaussian Quadrature, which requires that the integration be performed over a specific domain. This is the domain over which the master element is defined. This master domain is mapped to an

element's actual physical domain by the following formula

$$x_i(\xi,\eta,\zeta) = \sum_{m=1}^{n} x_i^{(m)} \psi^{(m)}(\xi,\eta,\zeta) \tag{2.46}$$

$x_i^{(m)}$ represents the physical coordinates of the m^{th} node of the element, and $x_i(\xi,\eta,\zeta)$ is the set of physical coordinates that correspond to the coordinates (ξ,η,ζ) on the master element. Note that this formulation is isoparametric, that is to say the spatial approximation over the element matches the approximation for the displacement over the element.

It can be noted from Eq. (2.33) and Eq. (2.37) that the calculation of the element stiffness matrix requires integrating the spatial derivatives of the basis functions in the physical domain. However, This integration must be carried out in the master element domain, and the basis functions are defined in terms of the master element coordinates. A transformation of these derivatives is therefore necessary. By the chain rule, Eq. (2.46) yields the following relationship between basis function spatial derivatives in the physical and master domains.

$$\begin{pmatrix} \frac{\partial \psi^{(m)}}{\partial \xi} \\ \frac{\partial \psi^{(m)}}{\partial \eta} \\ \frac{\partial \psi^{(m)}}{\partial \zeta} \end{pmatrix} = \begin{pmatrix} \frac{\partial x}{\partial \xi} & \frac{\partial y}{\partial \xi} & \frac{\partial z}{\partial \xi} \\ \frac{\partial x}{\partial \eta} & \frac{\partial y}{\partial \eta} & \frac{\partial z}{\partial \eta} \\ \frac{\partial x}{\partial \zeta} & \frac{\partial y}{\partial \zeta} & \frac{\partial z}{\partial \zeta} \end{pmatrix} \begin{pmatrix} \frac{\partial \psi^{(m)}}{\partial x} \\ \frac{\partial \psi^{(m)}}{\partial y} \\ \frac{\partial \psi^{(m)}}{\partial z} \end{pmatrix} = \boldsymbol{J} \begin{pmatrix} \frac{\partial \psi^{(m)}}{\partial x} \\ \frac{\partial \psi^{(m)}}{\partial y} \\ \frac{\partial \psi^{(m)}}{\partial z} \end{pmatrix} \tag{2.47}$$

where $\boldsymbol{J}$ is the Jacobian matrix. As noted, however, the inverse relationship is needed. The spatial derivatives of the basis functions must be expressed as derivatives with respect to the master coordinates. The spatial derivatives of the physical coordinates with respect to the master coordinates can easily be determined by differentiating Eq. (2.46), but the spatial derivatives of the master coordinates with respect to the physical coordinates are required. These derivatives make up the inverse of the

Jacobian.

$$\begin{pmatrix} \frac{\partial \psi^{(m)}}{\partial x} \\ \frac{\partial \psi^{(m)}}{\partial y} \\ \frac{\partial \psi^{(m)}}{\partial z} \end{pmatrix} = \begin{pmatrix} \frac{\partial \xi}{\partial x} & \frac{\partial \eta}{\partial x} & \frac{\partial \zeta}{\partial x} \\ \frac{\partial \xi}{\partial y} & \frac{\partial \eta}{\partial y} & \frac{\partial \zeta}{\partial y} \\ \frac{\partial \xi}{\partial z} & \frac{\partial \eta}{\partial z} & \frac{\partial \zeta}{\partial z} \end{pmatrix} \begin{pmatrix} \frac{\partial \psi^{(m)}}{\partial \xi} \\ \frac{\partial \psi^{(m)}}{\partial \eta} \\ \frac{\partial \psi^{(m)}}{\partial \zeta} \end{pmatrix} = \boldsymbol{J^{-1}} \begin{pmatrix} \frac{\partial \psi^{(m)}}{\partial \xi} \\ \frac{\partial \psi^{(m)}}{\partial \eta} \\ \frac{\partial \psi^{(m)}}{\partial \zeta} \end{pmatrix} \tag{2.48}$$

The partial derivatives of the master coordinates with respect to the physical coordinates (such as $\frac{\partial \xi}{\partial x}$) cannot be calculated directly from Eq. (2.46) to allow direct computation of $\boldsymbol{J}^{-1}$, so instead, the Jacobian will be calculated and then inverted. By differentiating Eq. (2.46) with respect to the master coordinates, the Jacobian is found to be the following

$$J_{ij} = x_j^{(m)} \frac{\partial \psi^{(m)}}{\partial \xi_i} = \begin{pmatrix} \sum_{m=1}^{n} x^{(m)} \frac{\partial \psi^{(m)}}{\partial \xi} & \sum_{m=1}^{n} y^{(m)} \frac{\partial \psi^{(m)}}{\partial \xi} & \sum_{m=1}^{n} z^{(m)} \frac{\partial \psi^{(m)}}{\partial \xi} \\ \sum_{m=1}^{n} x^{(m)} \frac{\partial \psi^{(m)}}{\partial \eta} & \sum_{m=1}^{n} y^{(m)} \frac{\partial \psi^{(m)}}{\partial \eta} & \sum_{m=1}^{n} z^{(m)} \frac{\partial \psi^{(m)}}{\partial \eta} \\ \sum_{m=1}^{n} x^{(m)} \frac{\partial \psi^{(m)}}{\partial \zeta} & \sum_{m=1}^{n} y^{(m)} \frac{\partial \psi^{(m)}}{\partial \zeta} & \sum_{m=1}^{n} z^{(m)} \frac{\partial \psi^{(m)}}{\partial \zeta} \end{pmatrix} \tag{2.49}$$

Note that for the inversion of the Jacobian to be possible, its determinant cannot be zero at any point in the element.

3. Numerical Integration

With a method for obtaining the derivatives of the basis functions with respect to physical coordinates, it is now possible to perform the stiffness matrix integration of Eq. (2.37) over the master domain using Gaussian Quadrature. Gaussian quadrature is based on the principle that the following relationship is exact for polynomials $f(\xi)$ of degree $2n-1$ or less, provided an appropriate selection of points ξ_i and weights w_i.

$$\int_{-1}^{1} f(\xi)\, dx \approx \sum_{i=1}^{n} w_i f(\xi_i) \tag{2.50}$$

Table II. Points ξ_i and weights w_i for various orders of Gaussian quadrature

n	ξ_i	w_i
1	0	2
2	$\pm\sqrt{1/3}$	1
3	0	$\frac{8}{9}$
	$\pm\sqrt{3/5}$	$\frac{5}{9}$
4	$\pm\sqrt{\left(3-2\sqrt{6/5}\right)/7}$	$\frac{18+\sqrt{30}}{36}$
	$\pm\sqrt{\left(3+2\sqrt{6/5}\right)/7}$	$\frac{18-\sqrt{30}}{36}$

The selection of points ξ_i and weights w_i is conducted using Legendre polynomials $P_n(\xi)$. These polynomials are given by the following equation

$$P_n(\xi) = \frac{1}{2^n n!}\frac{d^n}{d\xi^n}\left[\left(\xi^2-1\right)^n\right] \tag{2.51}$$

To start, $P_n(\xi)$ is normalized to give $P_n(1) = 1$. Point ξ_i is the i^{th} root of $P_n(\xi)$. The weight is given by the following relation.

$$w_i = \frac{2}{\left(1-\xi_i^2\right)\left(P_n'(\xi_i)\right)^2} \tag{2.52}$$

Table II gives the points and weights for a number for different quadrature schemes. Integration over three dimensions is simply the result of multiple one dimensional integrations, where the points are simply tensor-products of the one dimensional formulation. The integral of Eq. (2.37) is transformed to the master domain for

evaluation, resulting in

$$\begin{aligned}\boldsymbol{K} &= \int_{\Omega_e} \left(\boldsymbol{B}^{\mathrm{T}}\boldsymbol{C}\boldsymbol{B}\right) d\Omega_e \\ &= \int_{\hat{\Omega}_e} \left(\boldsymbol{B}^{\mathrm{T}}\boldsymbol{C}\boldsymbol{B}\right) |\boldsymbol{J}| d\hat{\Omega}_e \\ &= \int_{-1}^{1}\int_{-1}^{1}\int_{-1}^{1} \left(\boldsymbol{B}^{\mathrm{T}}\boldsymbol{C}\boldsymbol{B}\right) |\boldsymbol{J}|\, d\xi\ d\eta\ d\zeta\end{aligned} \tag{2.53}$$

where $\hat{\Omega}_e$ is the master domain of the element and $|\boldsymbol{J}|$ is the determinant of the Jacobian matrix. One final step remains to permit the integration of the element stiffness matrix. The strain-displacement matrix $\boldsymbol{B}$ of Eq. (2.33) contains the spatial derivative of the basis functions $\psi^{(m)}$ with respect to the physical coordinates, but the basis functions are defined in terms of the master coordinates. Therefore, the elements of $\boldsymbol{B}$ must undergo the following transformation outlined in Eq. (2.48), that is

$$\frac{\partial \psi_\alpha}{\partial x_i} = J_{ij}^{-1}\frac{\partial \psi_\alpha}{\partial \xi_j} \tag{2.54}$$

where ξ_i represents the master coordinates.

Finally , the element force vector is calculated by transforming the integration of Eq. (2.40) to the master domain as follows

$$\begin{aligned}f_\alpha &= \int_{\Gamma_e} \left(T_i \frac{\partial u_i}{\partial q_\alpha}\right) d\Gamma_e + \int_{\Omega_e} \left(\rho b_i \frac{\partial u_i}{\partial q_\alpha}\right) d\Omega_e \\ &= \int_{\hat{\Gamma}_e} \left(T_i \frac{\partial u_i}{\partial q_\alpha}\right) |\boldsymbol{J}| d\hat{\Gamma}_e + \int_{\hat{\Omega}_e} \left(\rho b_i \frac{\partial u_i}{\partial q_\alpha}\right) |\boldsymbol{J}| d\hat{\Omega}_e\end{aligned} \tag{2.55}$$

The element stiffness matrices and force vectors for all elements of the model are then combined through the process of assembly into a global system which is solved for nodal displacements using any number of schemes for solving symmetric-positive-definite linear systems.

E. Post-processing

Once nodal displacements are determined, the displacement at any location can be calculated via the Galerkin approximation by

$$u_i = \sum_{m=1}^{n} u_i^{(m)} \psi^{(m)} \tag{2.56}$$

These displacements can now be used to calculate strain by the relationship specified in Eq. (2.34). It ends up that the error reaches a minimum at the points used for Gaussian quadrature, so strain is calculated at these locations. Once strain has been calculated at a point, the stress at that point can be determined using the constitutive relationship of Eq. (2.10). These quadrature point stresses are used to examine failure criteria at the quadrature points. For plotting field data which is calculated at quadrature points, the field values are extrapolated to the nodes of the element. Then, nodal averages are taken between adjacent elements with the same material. Discontinuities are generally permitted across material interfaces, meaning that nodes on interfaces generally possess one value of the field variable for each material type with a boundary at that node. These nodal averaged field values are then used to generate a contour plot visualizing the field.

CHAPTER III

CONTINUUM DAMAGE MECHANICS

There are two major aspects to the continuum damage mechanics model. The first is the criteria which is used to determine when failure occurs in a material. For composite materials, it is also necessary to identify what kind of failure has occurred. The second aspect of the CDM model is the degradation scheme used to degrade material properties. Material properties are degraded according to the nature of the damage which exists due to the failure in an attempt to cause the degraded region to have an overall response matching a region containing discrete defects.

A. Failure Criteria

Because of the wide variety of failure modes which can occur in composites, predicting failure is a challenging problem. For isotropic materials, Tresca and Von Mises failure criteria are the the primary models used for predicting failure. For composites, however, there is a much larger variety of failure criteria which are widely used. Models such as Tsai-Hill, Hoffman, and Tsai-Wu examine the combined effect of stress components to predict failure. However, the increased accuracy which is obtained by examining the contribution of multiple stress components also makes it difficult to determine which component of stress is primarily responsible for causing failure. Therefore, these models are not optimal for systematic use in CDM.

The maximum stress failure criterion does not examine the combined effect of multiple components of stress. However, it clearly identifies the component of stress which causes failure. In addition, its simplicity makes it a good choice for quickly calculating failure. In its complete form, the max stress criteria predicts that a composite material has failed when one of the following inequalities are satisfied.

$$\begin{aligned} \sigma_1 > X_t \quad \sigma_2 > Y_t \\ \sigma_1 < X_c \quad \sigma_2 < Y_c \\ \tau > |S_s| \end{aligned} \tag{3.1}$$

where X_t and X_c are the tensile and compressive longitudinal strengths, respectively, Y_t and Y_c are the tensile and compressive transverse strengths, respectively, and S_s is the shear strength. If compressive and tensile strengths are taken to be equal and opposite, then material strengths can be expressed as a tensor S_{ij} with components corresponding to those in the stress tensor. Given this strength tensor, it is convenient to define a parameter called the failure index, FI, as follows.

$$FI = \left| \frac{\sigma_{ij}}{S_{ij}} \right| \tag{3.2}$$

Given this definition, a material is predicted to fail when $FI > 1.0$ for any component of stress. This method works best for models in which compressive stresses are mostly absent, as compressive and tensile failure vary significantly for composite materials.

B. Constitutive Degradation Model

The complex structure of composite materials means that the material response varies significantly across various failure modes. For instance, a composite which contains matrix cracking due to excessive transverse loading can still possess high stiffness in the fiber direction so long as the fibers have not failed. This leads to the necessity for development of a degradation scheme that affects constitutive properties differently for different composites. To develop such a scheme, one must first examine the various failure modes which can occur in composites, which are illustrated in figure 4.

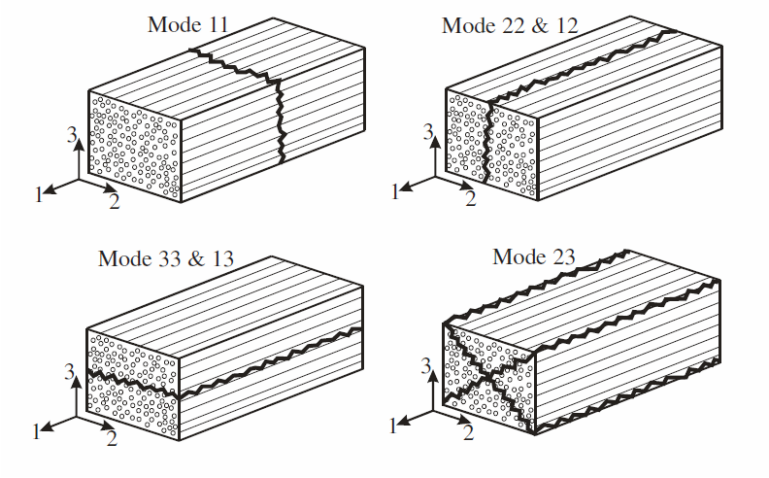

Fig. 4. Composite failure modes

A variety of models have been developed to address the issue of how various types of damage affect overall material response. Some of these include models proposed by Murakami and Ohno [2], Murikami [3], Blackketter et al. [7], Chapman and Whitcomb [8], Choiy and Tamma [11], and Zako et al. [10]. In many of these models, damage is represented by either a vector or a tensor which operates upon the material stiffness or compliance tensor. To facilitate the implementation of a variety of models in a single framework, the degradation schemes have been expressed in terms of degradation of engineering constants. These models are very similar with regards to which constitutive properties are degraded for a particular failure mode. They vary primarily according to how much the constitutive properties are degraded. The work performed in [1] utilized the Murakami-Ohno model of [2]. This work determined that the spurious behavior noted for prediction of damage due to shear stress by CDM was not improved by modification of the degradation model, leading to the conclusion that the particular constitutive degradation model selected does not contribute to the problems associated with CDM. While this was not explicitly investigated in the current work, it was supported by the fact that similar incorrect

predictions for damage growth were observed when using a damage model that was not the Murikami model. In the current work, the Blackketter model of [7] is utilized. The Blackketter scheme, expressed as a reduction of engineering constants, is shown in table III.

Table III. Blackketter degradation factors

Failure Stress	Engineering Constant to Degrade								
	E_1	E_2	E_3	G_{12}	G_{23}	G_{13}	ν_{12}	ν_{23}	ν_{13}
σ_{11}	100	100	100	100	100	100	100	100	100
σ_{22}	1	100	1	5	5	1	1	100	1
σ_{33}	1	1	100	1	5	5	1	1	1
σ_{12}	1	100	1	100	1	1	1	100	1
σ_{23}	1	100	100	100	100	100	1	100	1
σ_{13}	1	1	100	1	5	100	1	1	1

In the current implementation damage either exists completely or does not exist for a particular mode - there is no "in-between" state of partial damage for a given stress component. If, after one mode of damage occurs, an additional mode occurs that results in a more severe damage factor for one of the engineering constants, then the degradation factor is increased to the value for the new damage mode.

C. Implementation

For the analyses performed in this research, the continuum damage mechanics model was implemented in a linear finite element framework. Applied displacements were

1. Perform linear analysis
2. Scale load and solution vector such that the maximum failure index at any quadrature point in the model is 1.001 to ensure that new failure occurs
3. Iterate at constant load to achieve equilibrium as follows
   (a) Identify quadrature points with failure using the max stress failure criterion
   (b) If no quadrature points are in failure, the model is in equilibrium and iteration is ended (go on to step 4)
   (c) Degrade the properties at failed quadrature points by dividing the engineering constants by the appropriate degradation factors
   (d) Perform linear analysis
   (e) Return to step (a)
4. Return to step 2 until the desired load is reached

Fig. 5. Algorithm for CDM implementation in FEA

small, resulting in volume average strains not exceeding 1%. The algorithm for implementation is given in figure C.

CHAPTER IV

CONFIGURATIONS

A variety of numerical experiments were performed, primarily to investigate the major issue which was not examined in the research performed by Gorbatikh et al. [1] - the effect of the geometry of the initially damaged region. Only two damaged geometries were examined in [1], a discrete crack and a circular degraded region. Understandably, a circular region represents a general inclusion without any directional bias in its shape, and it is conducive to obtaining an analytical elasticity solution. However, there are several issues to be addressed regarding the selection of a circular region for comparison to a crack by way of an analytical elasticity solution. First, except for a few very specialized implementations, there are no circular elements in finite elements. Second, in the progression of an analysis using CDM the damaged region will obtain a shape which will most likely possess some directional bias instead of being circular. Finally, the elasticity solution can only identify where new damage will initiate around the existing circular degraded region. It cannot predict the overall shape that the damage zone will evolve into as loading is increased and the damage zone grows.

In investigating the effect of the initially degraded geometry on the resulting damage zone, four configurations were investigated. Each investigates a different aspect of the shape of the degraded region. The configurations investigated were an initial discrete crack, an elliptical hole, an elliptical inclusion, and a row of degraded elements. Each of these configurations attempts to address at least one of the issues with using a circular inclusion in comparison to a discrete crack. Furthermore, different loadings are examined which result in different types of shear stress concentrations around the initially damaged region.

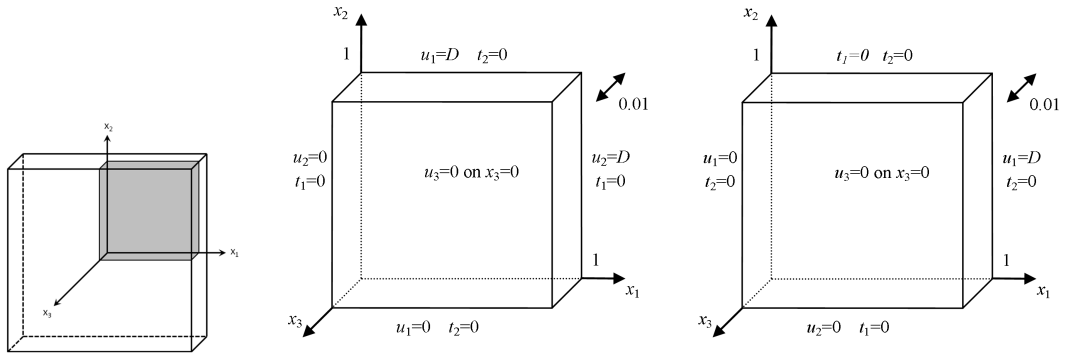

(a) **(b)** **(c)**

Fig. 6. Overall model geometry **(a)** analyzed region **(b)** shear load BCs **(c)** tensile load BCs

A. Model Geometries

In general, the models represent one eighth of a thin plate. Symmetry and anti-symmetry conditions are utilized to reduce model size. Two general loading cases are examined, in-plane shear and fiber-direction tension. In all cases, loads are applied as specified displacements on the boundaries. The general configuration of the model is shown in figure 6.

1. Discrete Crack

The first model examined possesses an initial discrete crack in the mesh. This geometry should provide the most accurate representation of the stress state which would exist around an actual crack that can be obtained using FEA, provided that the mesh is sufficiently refined. Such a model serves as a useful test for CDM. If CDM cannot correctly predict the growth of a damage zone when provided a stress state that very closely corresponds to that found around an actual crack, then it is unlikely that any other initially damaged geometry for which the nature of the damage is not distributed micro-defects would result in CDM making an accurate prediction of

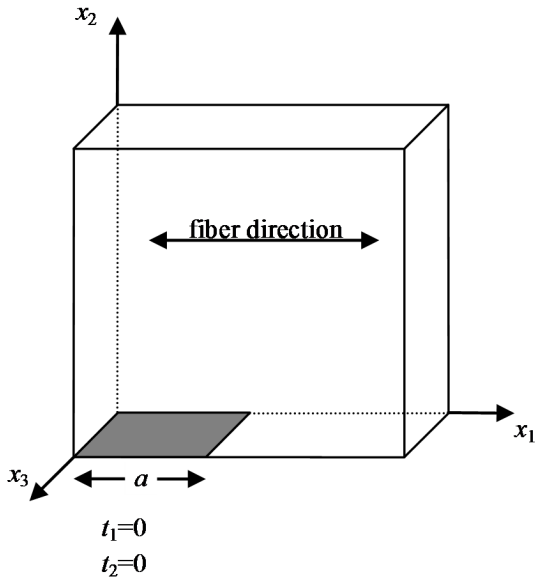

Fig. 7. Discrete crack model geometry

damage growth.

To introduce a crack into the model, a portion of the anti-symmetry or symmetry (depending on the loading) boundary condition was replaced with a traction free boundary condition as shown in figure 7. This model for a discrete crack is somewhat simplified in that crack surface inter-penetration is not prevented, nor is crack surface friction accounted for. A variety of crack lengths $2a$ were investigated, both running along the fiber direction (for plates under shear load) and running transverse to the fibers (for plates under fiber-direction tensile load). Mesh refinement in these models was varied to identify mesh dependencies on the result. For all models, the elements along the crack surface and near the tip are square, and elements away from the crack are as close as possible to square.

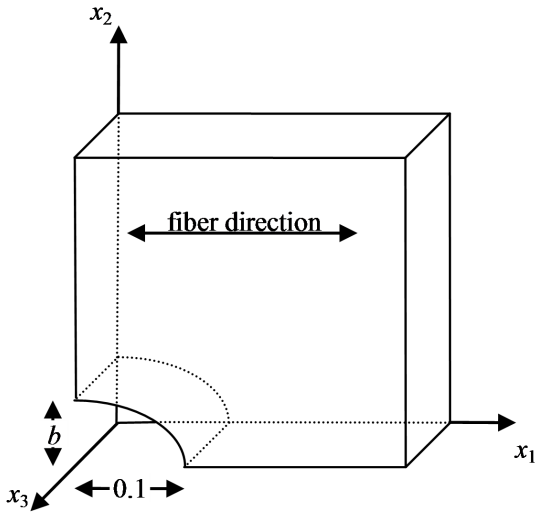

Fig. 8. Elliptical hole model geometry

2. Elliptical Hole

Like a crack, a hole in a plate represents a form of discrete damage. For uniaxial composites under tension, holes result in the formation of a well-documented H pattern of damage resulting from local shear stress concentrations. Therefore, a variety of hole models, as shown in figure 8, were run to determine if CDM is able to correctly predict the development of such an H pattern of damage. Also, a hole could be considered to represent a region degraded using a primitive degradation model in which all stiffness is eliminated without regard for the stress which caused the damage (essentially complete element death). Various hole eccentricities were examined to determine if the behavior of a hole approaches the behavior of a model with a discrete crack. The impact of mesh refinement was also examined.

3. Elliptical Inclusion

An elliptical inclusion was studied for the purpose of expanding upon the investigations of Gorbatikh et al.[1]. While in that work only a circular inclusion was inves-

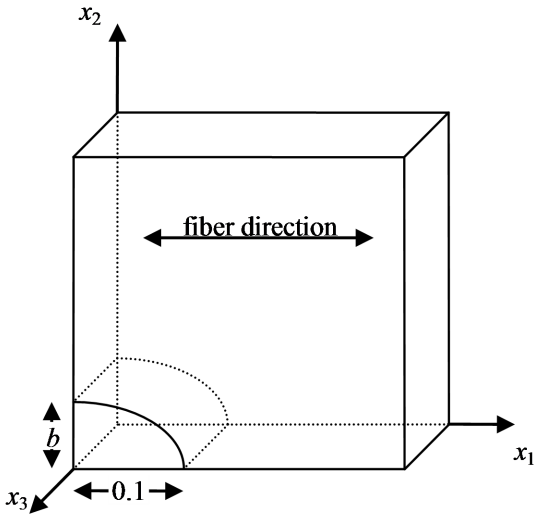

Fig. 9. Elliptical inclusion model geometry

tigated, this study aims to determine if the the eccentricity of the inclusion changes the overall shape of damage zone growth predicted by the CDM model. A number of ellipses were examined by varying b, the dimension of the minor axis. For all ellipses, a, the major axis dimension, was held constant to $1/10^{th}$ the model size as shown in figure 9. Results will be reported in terms of eccentricity, defined in Eq. (4.1)

$$e = \frac{\sqrt{a^2 - b^2}}{a} \tag{4.1}$$

4. Line of Degraded Elements

One issue regarding all of the geometries previously mentioned is that they all involve pre-existing damage with a well-defined geometry. Initially degraded regions can be described with highly refined meshes that yield results which closely match those obtained from an elasticity analysis (with the exception of the discrete crack which will not yield the infinite stress concentration predicted by elasticity due to the finite nature of the discretization). This situation varies greatly from the normal procedure

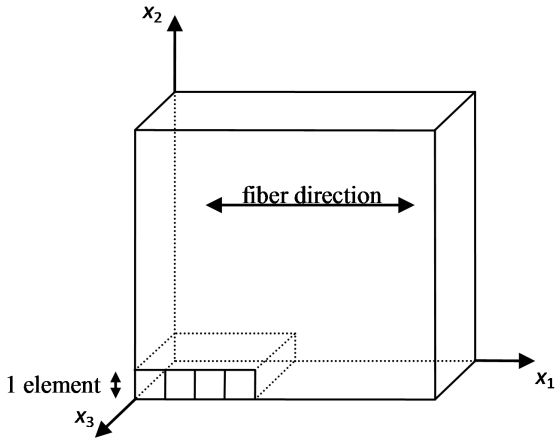

Fig. 10. Line of degraded elements model geometry

of a progressive damage analysis using CDM, however. In a such an analysis analysis, typically there will not be any initial damage. Instead, the damage zone will nucleate at most likely one quadrature point in the model and grow from that point. Therefore, early in the process of damage zone growth the damage zone will be represented very coarsely by the mesh since it will most likely encompass only one or a few elements. Also, at its initial formation, its shape will depend wholly upon the shape of the element where damage first occurs. Therefore, one other type of geometry was examined. This geometry is a uniform mesh with just one or a few degraded elements, generally arranged in a row as shown in figure 10. Various patterns were examined to determine if CDM can correctly predict damage zone growth provided sufficient directional bias in a degraded region with low mesh refinement.

B. Material Properties

The material properties utilized for this analysis are those utilized by Guagliano and Riva [12] and are given in table IV. Orthotropic properties are assumed throughout the analysis. It has been observed that damage in composites occurs either aligned

with or orthogonal to the fibers, meaning that the symmetries of Eq. (I) remain valid after damage has occurred, and the material therefore remains orthotropic.

Table IV. Material properties of homogenized carbon fiber-matrix

Moduli		Strengths	
E_1	165 GPa	S_{11}	2550 MPa
E_2, E_3	9.95 GPa	S_{22}	152 MPa
G_{12}, G_{13}	7.26 GPa	S_{33}	152 MPa
G_{23}	3.9 GPa	S_{12}	97 MPa
ν_{12}, ν_{13}	0.24 GPa	S_{23}	55 MPa
ν_{23}	0.5 GPa	S_{13}	97 MPa

CHAPTER V

RESULTS

A. Discrete Crack

Applying traction-free boundary conditions along part of the surface of symmetry introduces a discrete crack into the mesh. As mesh refinement around the crack is increased, the stress state in the vicinity of the crack more closely matches the stress predicted by elasticity. As the failure criteria for the CDM implementation is based upon stress, it is hypothesized that the stress distribution around an actual crack will result in an accurate prediction for the growth of the damage zone. If this is not the case, then there is little possibility that CDM could correctly predict damage zone growth around an initial damage zone that only somewhat approximates an actual crack for the same loading.

1. Initial Crack Along Fibers Under Shear Loading

In [1], it was predicted that for a unidirectional composite containing a crack running along the fiber direction under shear stress, crack growth would occur along the fiber direction since this is the direction requiring the lowest energy release rate. In such a situation, the fibers serve to arrest crack growth in the transverse direction, allowing only matrix cracking to accumulate running along, but not crossing, the fibers. Since CDM does not model cracks discretely, it will be deemed successful in predicting damage growth for this case if it predicts a narrow band of damaged elements initiating at the tip of the discrete crack and growing along the fiber direction.

It was found that as mesh refinement is increased, CDM correctly predicts damage zone growth for a discrete fiber-direction crack under shear load. Insufficient mesh

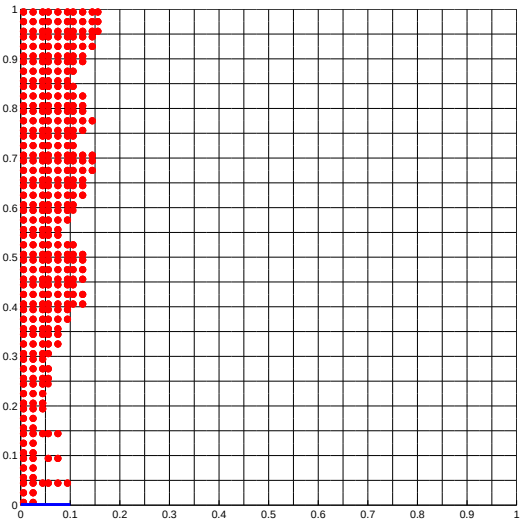

Fig. 11. Discrete crack under shear, 400 elements, $a = 0.1$

refinement yields wholly inaccurate results as seen in figure 11. In this case, CDM predicted that damage grew in the x_2 direction, contrary to the predicted behavior. As mesh refinement is increased as in figure 12, the model begins to behave in a more correct fashion, although some spurious damage growth in the x_2 direction is still predicted. Further increase of mesh refinement, however, yields damage growth in the x_1 direction only, matching the predicted behavior as seen in figure 13. For shorter cracks ($a < 1/10$) , it was found that six or more elements along the crack length yielded an accurate prediction. For longer cracks, seven elements along the crack length were required to obtain correct results. These findings support the hypothesis that the if provided a sufficiently accurate stress field, CDM can correctly predict the direction of damage zone growth.

It may be noted for the previous models that the damage zone extends into the elements along the crack surface. This surface, however, is traction free, and therefore

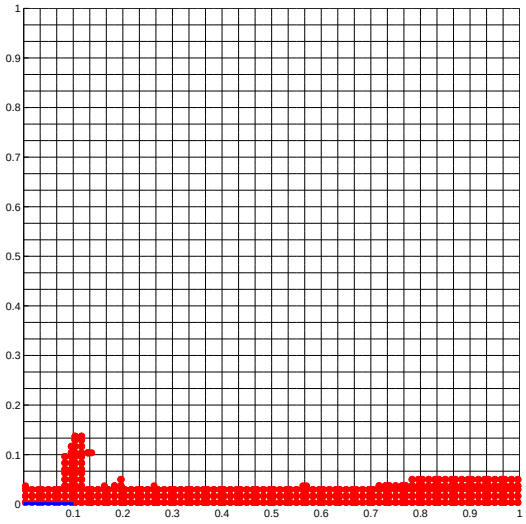

Fig. 12. Discrete crack under shear, 900 elements, $a = 0.1$

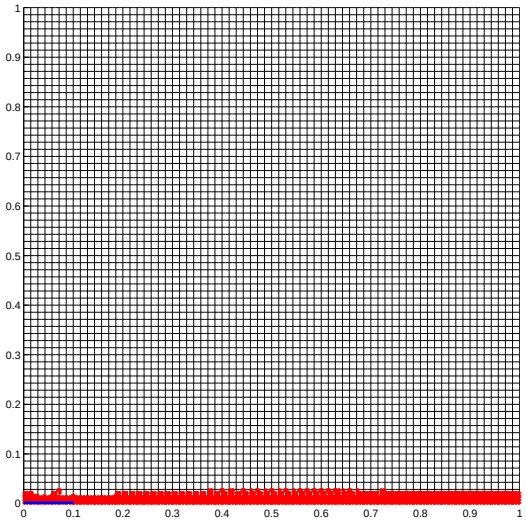

Fig. 13. Discrete crack under shear, 4900 elements, $a = 0.1$

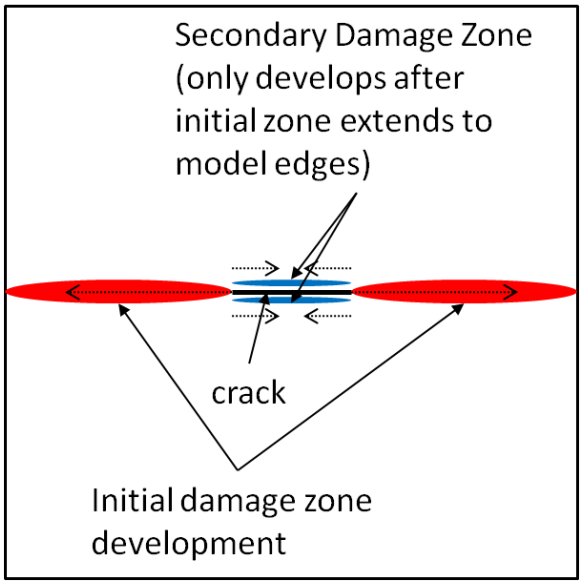

Fig. 14. Progression of damage zone for discrete crack

it would be expected that no damage would occur in this location. To address this issue, it is important to understand the progression of the damage zone. In all of these cases, the shown damage zone occurred in a single load step. In all cases, on an iteration-by-iteration basis, damage initiated at the tip of the crack and proceeded to grow away from the crack tip all the way to the edge of the model as shown in figure 14. At this point, the model is essentially completely failed as the combined crack and damage zone span the entire mesh. However, because the damaged material still possesses stiffness to x_1 direction tensile load (note in table III that E_1 is not degraded for failure due to σ_{12}), the model is still able to carry some load. This leaves the elements along the crack surface as the primary load path, and they in turn fail starting at the crack tip moving along the crack surface. So, although this region should be damage free, the presence of damage here is not an issue of concern as it occurs only after the model has completely failed in a logical manner.

2. Initial Crack Transverse to Fibers, Fiber Direction Tensile Loading

Cracks which run transverse to the fiber direction for composites behave differently under fiber direction tension than they would in a metal. Near the crack tip, there exists a concentration of both σ_{11} and σ_{12}. In a composite, the elevated σ_{12} causes failure as S_{12} is typically significantly lower than S_{11}. The result is the development of damage zones which initiate at the crack tip and grow along the fiber direction as the matrix joining the strip of material containing fibers cut by the crack and the remainder of the composite structure fails under shear stress. The resulting H pattern of damage has been extensively obseerved both experimentally [13] and through numerical analysis [3].

This configuration was tested using CDM to predict the growth of the damage zone. In all cases tested, the shear stress concentration around the crack resulted in a damage zone which began at the crack tip and ran along the fiber direction to the opposite edge of the model before damage zone growth transverse to the fibers began, as seen in figure 15. This result was independent of the mesh refinement relative to the crack length, and matched the behavior observed for composites exactly. This result further supports the belief that CDM can accurately predict damage growth when provided with an accurate stress field, and also shows that CDM is able to accurately predict damage growth when the damage occurs due to a shear stress concentration resulting from some defect under a global tensile load.

B. Elliptical Hole

While an elliptical hole represents discrete damage, it does not result in singular stress concentrations as a crack does (provided the ellipse eccentricity is not approaching a limit of 1). The location of the greatest shear stress concentration between an

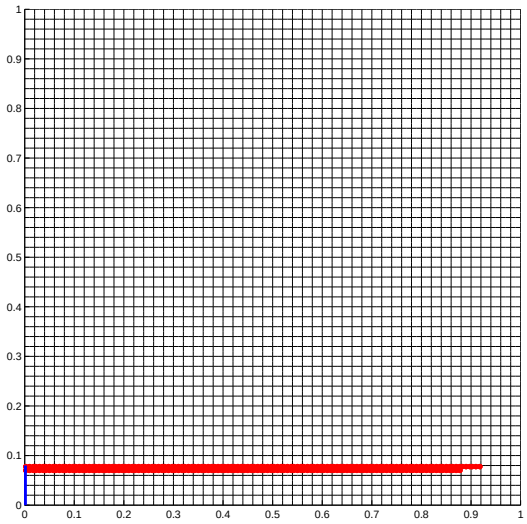

Fig. 15. Damage zone for transverse crack under tension

elliptical hole and a crack varies significantly as well. For a crack, the shear stress reaches a maximum at the tip on the x_1 axis for a crack running along the fiber direction. For a traction-free elliptical hole centered at the origin, however, equilibrium requires that the shear stress where the hole meets the x_1 axis be zero.

Both shear loading and fiber-direction tensile loading were examined. For the case of shear loading, the expected behavior is local failure due to elevated σ_{12} or σ_{22} (the stress causing failure depends on material properties) on the hole surface which progresses along the fiber direction. For the case of fiber-direction tension, damage should initiate at the maximum σ_{12} concentration on the hole near the x_2 axis (but not on it), and then grow along the fiber direction, forming an H pattern similar to that observed for a crack [13].

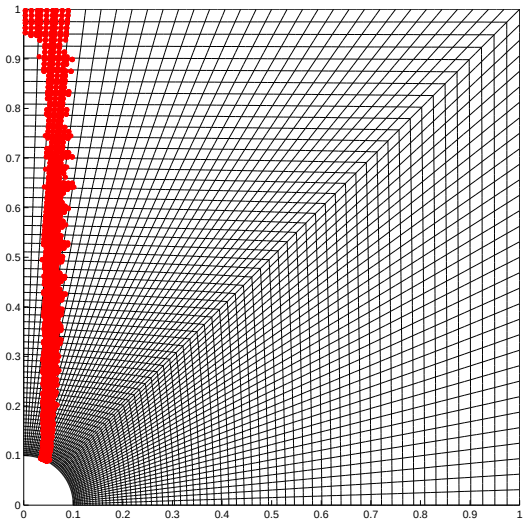

Fig. 16. Damage zone for elliptical hole under shear, eccentricity = 0

1. Shear Loading

For models with a circular hole under global shear load, the damage zone initiated on the hole at the location of maximum σ_{12} and immediately began growing in the x_2 direction, transverse to the fibers, as seen in figure 16. This damage growth behavior does not match the physical realities of composite materials, but does match the spurious behavior noted by Gorbatikh et al. [1] as well as the damage growth the CDM predicted for an elliptical inclusion, reported in the following section. Furthermore, this behavior was found to be mesh independent for a circular hole.

In order to study the effect of the hole's shape on predicted damage growth, holes with a variety of eccentricities were examined in the hope that a sufficiently flat ellipse could correctly predict damage growth. It was found that as eccentricity increased and approached 1, the shear stress concentration moved closer and closer to the x_1 axis. However, provided that the mesh around the ellipse tip was sufficiently

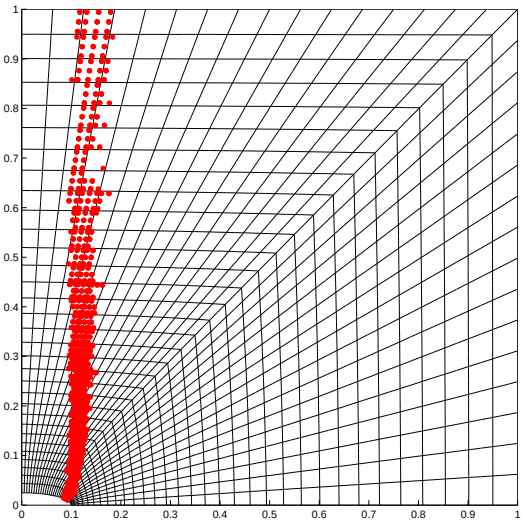

Fig. 17. Damage zone for elliptical hole under shear, eccentricity = 0.968

refined, the initial failure never occurred on the x_1 axis itself, and the damage zone grew transverse to the fibers (in the x_2 direction), as seen in figure 17.

There was a peculiar mesh dependence observed for this model. It was noted that if the refinement near the tip of the ellipse was reduced, eventually the initial damage location moved from the ellipse surface to a location a little ways off the ellipse tip but on the x_1 axis. From this initial failure, the damage zone proceeded to grow in the fiber direction. This does not suggest that the CDM model is accurately predicting damage growth in this situation because these "correct" results only occur when the stress field around the discrete damage is not accurately represented (due to the coarser mesh). This mesh dependence was also observed for models of elliptical inclusions with eccentricities approaching 1, and is described in greater depth in the section reporting results for those models.

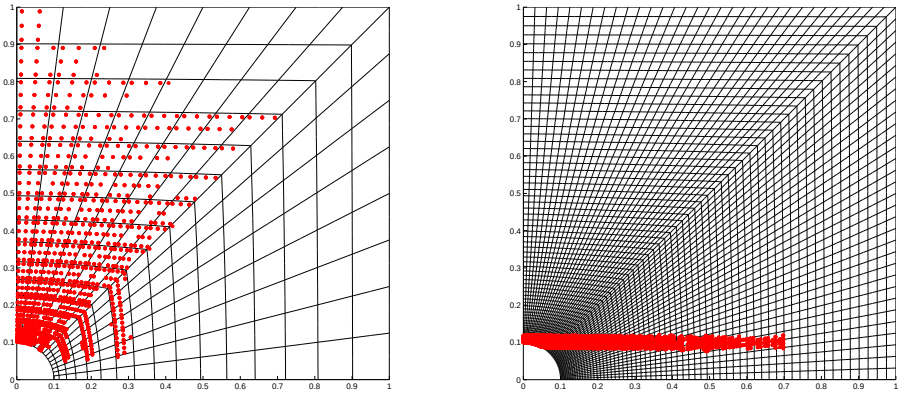

(a) **(b)**

Fig. 18. Damage zone for circular hole under tension **(a)** 256 elements **(b)** 4096 elements

2. Fiber-Direction Tensile Loading

A number of models of circular holes under fiber-direction tension were analyzed to determine if CDM could predict the development of the H pattern of damage for this initial defect as it could for a crack. The analyses showed that sufficient mesh refinement around the hole resulted in logical predictions for damage progression(figure 18). Furthermore, more refined meshes resulted in narrower damage zones that grew further along the fiber direction before transverse failure began to occur near the hole. These findings provide further support to the idea that CDM is able to effectively predict damage growth due to shear failure when the failure is due to a shear stress concentration resulting from a defect in the presence of global tensile stress.

C. Elliptical Inclusion

The third configuration examined was an elliptical inclusion. This most directly corresponds to the investigation conducted by Gorbatikh et al. [1], in which the

stress distribution around a circular degraded inclusion was investigated. In this investigation, two additional aspects are examined. The first is the effect of adding directionality to the degraded region. The second is to examine damage zone growth beyond its initiation ([1] only examined the location of initial damage occuring around the degraded region). Also, since this is a finite element analysis and not an analytical elasticity solution, the effect of mesh refinement is examined.

For this investigation, an elliptical inclusion was introduced into the mesh. Its properties were degraded according to the Blackketter model for failure due to σ_{12} (see table III). Like the investigation of an elliptical hole, several eccentricities were examined. As the eccentricity of the degraded region approaches 1, it becomes more and more crack like. While the interface of the degraded region is not traction free as it was for the hole, the shear stress on the interface near the x_1 and x_2 axes will be relatively low. This is because the degraded region has a low shear stiffness (G_{12} has been degraded by a factor of 100) and therefore will not carry significant shear loading at these locations (requiring that the adjacent material also have low shear stress to maintain equilibrium).

The first analysis performed was a linear elastic analysis of several inclusions of various eccentricities to determine the effect of shape on the location of the maximum stress concentration (figure 19). It was found that as the eccentricity was increased, the shear stress concentration (which for this case resulted in the highest failure index and therefore will be responsible for the initial failure) moved closer to the ellipse tip, but it never completely reached the ellipse tip. The model region adjacent to the inclusion tip and on the x_1 axis was found to be a region of low stress, although the stress rapidly increased to a local maximum a little ways away from the tip along the x_1 axis.

There was an interesting mesh dependence which was noted in the performance of

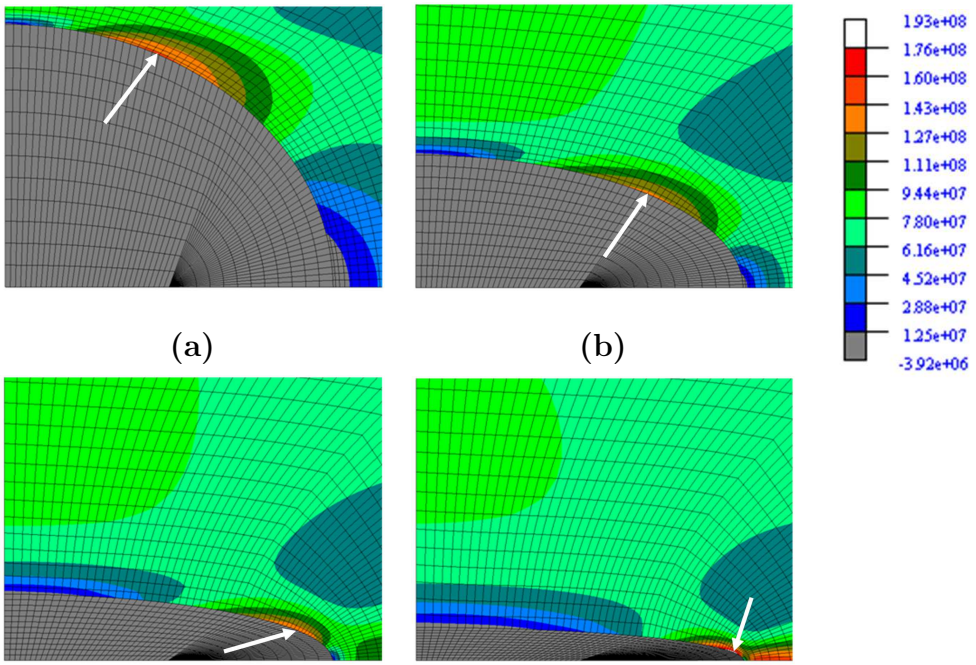

Fig. 19. Stress distribution around elliptical inclusion (maximum noted) **(a)** $e = 0$ **(b)** $e = 0.866$ **(c)** $e = 0.968$ **(d)** $e = 0.992$

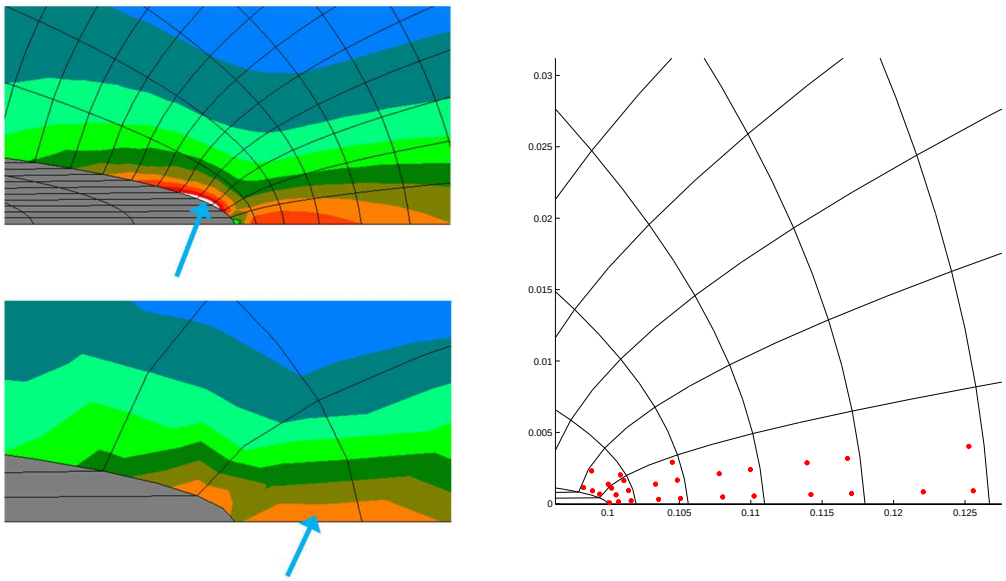

(a) **(b)**

Fig. 20. Mesh dependence observed for an elliptical inclusion **(a)** Stress concentration **(b)** Resulting damage zone growth

this investigation, shown in figure 20. Provided that mesh refinement around the tip of the ellipse was high enough, the maximum shear stress concentration was located on the inclusion interface no matter how close the eccentricity was to 1. However, for ellipses with high eccentricities, if the mesh refinement near the tip was reduced, the stress field around the inclusion was altered. In such cases, the stress concentration on the inclusion interface was reduced and the local maximum a little ways off the tip of the inclusion on the x_1 axis became the greatest stress concentration in the model.

It was found that for all models in which the mesh refinement was sufficient to result in a maximum stress concentration on the inclusion interface, the damage zone grew from this point of maximum stress transverse to the fibers (in the x_2 direction), contrary to the expected behavior, as seen in figure 21. This held true for ellipses of all eccentricities, provided that the mesh was sufficiently refined. In models with meshes which were coarse, resulting in the maximum stress concentration existing

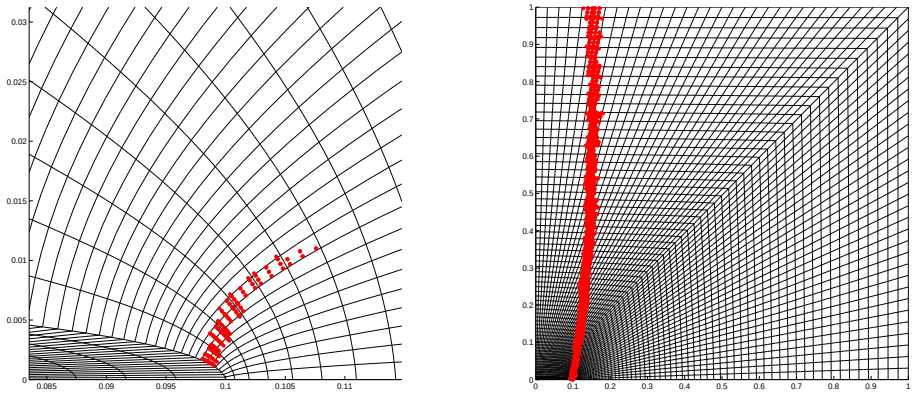

(a) **(b)**

Fig. 21. Damage zone growth for an elliptical inclusion with $e = 0.997$ **(a)** Early damage zone growth **(b)** Final damage zone growth

on the x_1 axis a little ways off the ellipse tip, the damage zone grew along the fiber direction as seen in figure 20. Although this behavior matches the expected behavior for a composite, it is considered spurious as it results from an inaccurate stress field. It is interesting to note in this case that "correct" behavior is obtained only when the mesh is not sufficiently refined to accurately represent the stress which exists in the model.

D. Line of Degraded Elements

All of the results discussed up to this point were obtained from models with clearly defined initial damage. While such investigations are useful for investigating the overall behavior of CDM in an attempt to model large-scale discrete defects, they are not truly representative of a typical analysis utilizing CDM. In such an analysis, damage will not initially exist in the model. The model load will be increased to the point that failure occurs at one location. Properties at that location will be

degraded and constant-load iterations will take place to restore equilibrium to the model. Since damage only occurs at a limited number of quadrature points, there will likely only be one or a few elements with degraded properties initially. The damage zone will therefore only be coarsely defined by the mesh, and its shape will largely be determined by the shape of the elements in which the initial damage occurs. To determine if CDM can correctly predict damage zone growth when the damage zone is only very coarsely represented by a few elements, a uniform mesh was created and a limited number of elements were degraded in the mesh.

1. Single Degraded Element

The first model which was investigated was a uniform mesh of square elements in which one element was degraded. Therefore, like the circular region from [1], this initially degraded region lacked any directionality in its geometry. This configuration was found to result in damage zone growth transverse to the fibers as seen in figure 22, contrary to the expected behavior but matching the behavior previously observed for other degraded regions lacking any geometric directionality.

To ensure that the element orientation itself was not affecting the results of this model, the material system and loading were both rotated 45°. The results from this analysis matched the unrotated case, with damage growing transverse to the fiber direction as shown in figure 23. These results combined with previous observations appear to indicate that without any directionality in the geometry of the damage, CDM cannot accurately predict the direction of damage zone growth for composites experiencing large-scale cracking due to shear failure. It also suggests that the material anisotropy actually drives the direction of predicted damage zone growth in the incorrect direction.

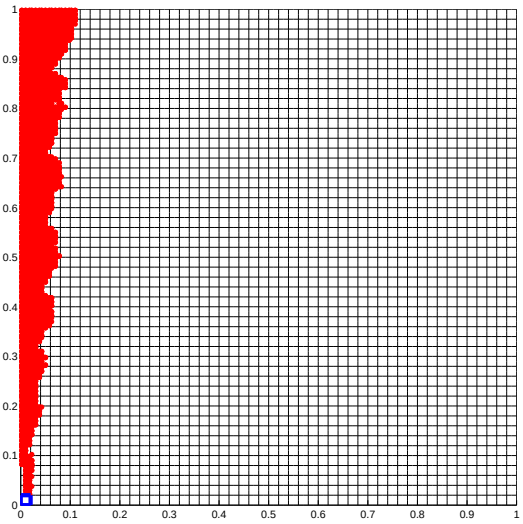

Fig. 22. Damage growth around a single degraded element

2. Multiple Degraded Elements

The next investigation was intended to determine if some directionality in a coarsely defined damaged zone could lead to correct damage zone growth predictions. For this analysis, a few elements in a row running along the x_1 direction were degraded. For the material properties given in table IV, it was determined that if a row of four or more uniform square elements were degraded in a mesh of 1600 square elements, CDM predicted damage zone growth along the x_1 direction as seen in figure 24. To further investigate the effect that shape played in influencing damage zone growth, the mesh was modified. The damage zone shape (a row of 4 square elements) was held constant, but different mesh refinements were tried. First, a model was run with elements with an aspect ratio of 4:1 such that the damaged zone occupied only one element. Next, a 6400 element mesh with uniform square elements was used. In this case, the damage zone occupied a region of 2 elements in the x_2 direction and 8

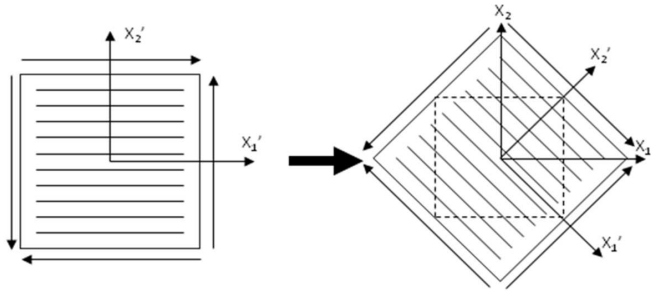

(a)

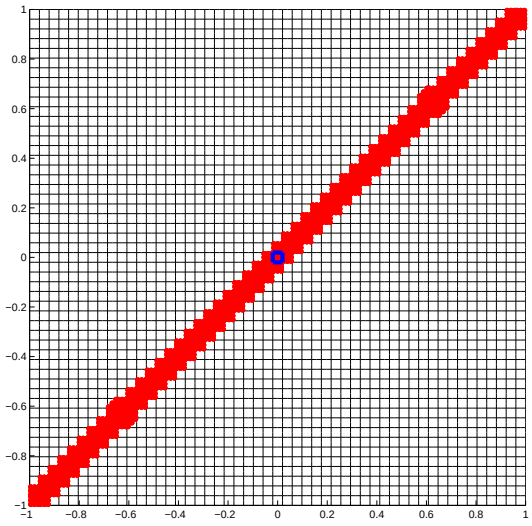

(b)

Fig. 23. Damage growth around a single degraded element, mesh rotated 45°

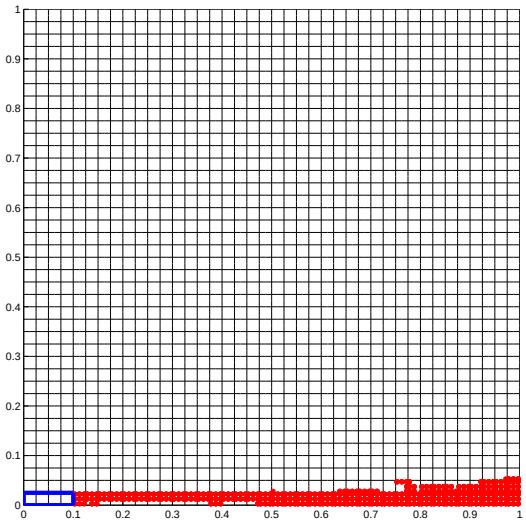

Fig. 24. Damage zone growth around damaged region with 4:1 dimensional ratio, 1600 elements

elements in the x_1 direction. Both of these meshes exhibited damage growth along the fibers, matching the predicted behavior for composites. This result indicates that for coarsely defined damage, sufficient directionality in the damage zone can lead to a correct prediction for damage zone growth, and that for low mesh refinement the shape of the damage zone is more important than the mesh refinement of the damage zone.

The effect of material anisotropy in driving the damage direction was further investigated by running a series of models with varying material properties. The properties were simply varied in a linear fashion between the properties for composites given in table IV to those characteristic of 2024-T4 Aluminum Alloy, an isotropic material with Young's Modulus E of 73.1 GPa, a Poisson Ratio ν of 0.33, and a tensile strength of 469 MPa. It was found that as the ratio between E_1 and E_2 reduced to 1, the length of the initially damaged region required to cause damage

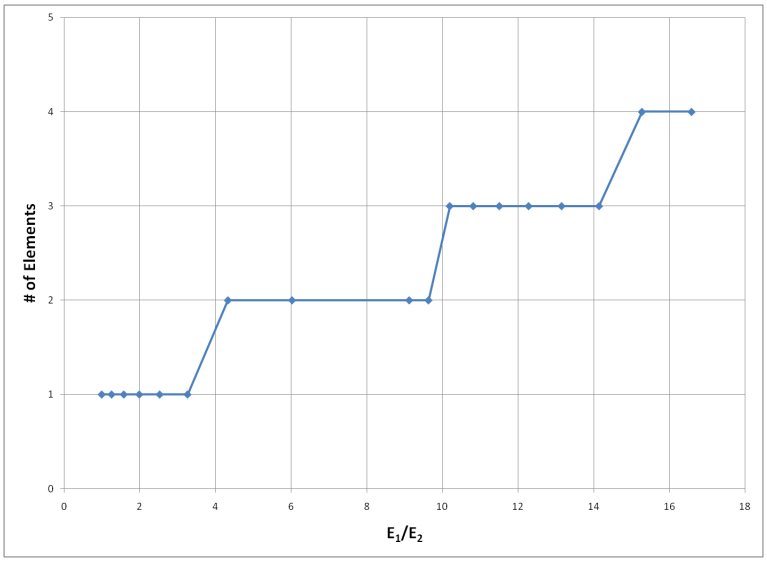

Fig. 25. Length of degraded region required for correct damage growth for varying anisotropy

to grow in the predicted direction decreased, eventually reaching the point where a single degraded element resulted in correct damage propagation for a material with $E_1/E_2 \approx 2.5$ (Figure 25). Although the degradation model's applicability to this fictitious material is dubious, the results of this investigation further support the idea that the material anisotropy found in composite materials is a significant contributor to CDM's inability to correctly predict damage under shear stress in the absence of sufficient directionality in the initially damaged region. Furthermore, the fact that materials with lower anisotropy exhibited correct damage zone growth with a single degraded element suggests that the degradation model tends to cause damage to grow in the expected direction, as these models had no directional bias in the region of initial damage.

CHAPTER VI

PREDICTIVE DEGRADATION MODEL

The results observed thusfar show that there are issues with utilizing CDM to predict the behavior of a composite which is experiencing large-scale cracking that cannot be considered in a continuum sense. However, it has also been shown that there are cases where CDM yields correct results even for damage it was not originally conceived to model. Due to its simplicity as a tool, as well as the complexity of accounting for a large number of cracks which can arise in complex composite architectures, it would be advantageous to identify some modification to the analysis overall that would cause CDM to generally better predict damage growth for these these probelmatic failure modes. Based on the results obtained from degrading a limited number of elements in a uniform mesh, it is observed that sufficient directional bias in the initially degraded region can cause the damaged region to grow in a manner that is logical for shear failure in a composite. However, one of the arguments for only degrading a small number of elements was that when damage initially occurs in a model, it generally will not occur with any particular directional bias. In order to exploit the findings of the previous section, some modification must be made to the algorithm for CDM which has been followed up to this point (figure C) to encourage the creation of an inital damage zone which possesses sufficient directionality to drive damage growth in a logical manner in subsequent load steps.

A. Method

In order create such a degraded region, an obvious approach is to somehow degrade elements around the element where failure initially occurs. The most straightforward method would be to directly degrade engineering constitutive properties in quadrature

points that lie in a certain geometry around the location of initial failure. Another method is to reduce the strength of quadrature points that lie within a certain geometry of the initially damaged region. This second option was chosen for further investigation as it leaves more flexibility in the model for damage to evolve in a variety of ways. The basic algorithm that was investigated is outlined in figure A.

Two issues must be considered for this modification of the CDM approach. The first is how large a region must be given degraded strengths. This issue, for the case of a uniform mesh in a 2D-esque configuration, is addressed by the investigation of a rows of degraded elements in chapter V, section D. A more extensive study would need to be performed to address three dimensional models and non-uniform meshes, but that is beyond the scope of this initial investigation. The second issue to be addressed is how much the strengths must be degraded within the identified region. The behavior exhibited in previous experiments suggests that this likely depends on the degree of material anisotropy, with higher anisotropy requiring greater degradation of strength to cause the formation of an inital damage zone which will result in logical damage zone growth.

In order to determine the nature of this dependency, a model was developed such that the strength of the central element was degraded to ensure it would fail before all others when the model was subjected to uniform shear stress. Immediately after this initial failure occurred, the failure indices of the surrounding elements were examined (Figure 27). The required strength degradation factor is determined in the following manner. First, the maximum failure index for shear stress in the element directly above the initially failed element (the element that represents incorrect damage growth, shaded yellow) is determined. Then, based on the material anisotropy and the findings reported in figure 25, the maximum failure index for shear stress is identified in each element that lies within the geometric zone which must be de-

1. Perform linear analysis
2. Scale load and solution vector such that the maximum failure index at any quadrature point in the model is 1.001 to ensure that new failure occurs
3. Check if damage already exists in some element adjacent to the element with a max failure index of 1.001
   (a) If no damage exists (meaning this is the start of a new damage zone) then do the following to create an initial damage zone with sufficient directionality for correct damage zone growth
      i. Degrade the constitutive properties of the failed quadrature points
      ii. Define a geometric region around the degraded quadrature points where failure is expected based on the failure mode
      iii. Degrade the strengths for the elements within this geometric region by some factor
   (b) If damage does already exist (this is an already existing damage zone that is growing) then utilize the iterative process in step three from figure C
4. Return to step 1 until the desired load is reached

Fig. 26. Modified algorithm for CDM implementation in FEA

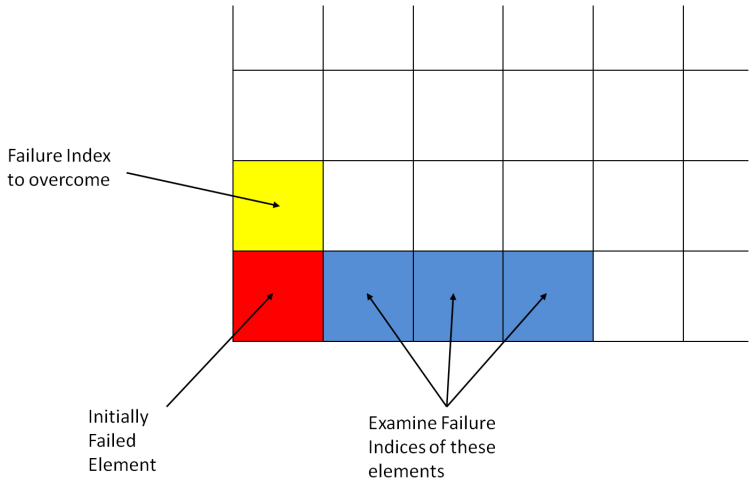

Fig. 27. Elements of interest in examining effects of anisotropy on required strength degradation

graded to cause correct damage zone growth (shaded blue). The required strength degradation factor is the number by which the strengths of these elements (the blue elements) would have to be divided so that all of their maximum failure indices exceeded the maximum failure index of the element above the initial damage (the yellow element). In other words, it represents how much the strengths must be degraded for the elements in the expected damage zone so that they fail before damage begins to grow in the incorrect direction. The findings are reported in figure 28. As expected, the required strength degradation factor exhibits a strong dependence on material anisotropy.

Again, these strength degradation factors apply only to a uniform mesh in a more-or-less 2D configuration. Also, it is certainly plausible that strength degradation factors lower than those shown in this study could result in the desired damage zone growth since the stress state, and therefore the failure indices, will change as the damage zone evolves from iteration to iteration.

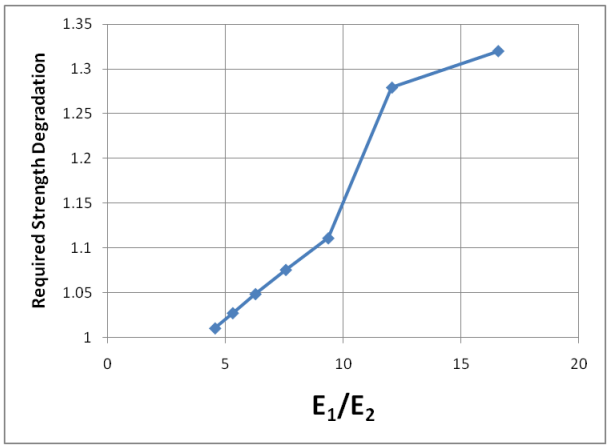

Fig. 28. Required strength degradation factors for various degrees of material anisotropy

B. Results From Method

Some experimentation was performed on a 20x20 uniform mesh using this modification to the CDM algorithm (Figure 29). The model used the proprieties for homogenized carbon fiber-matrix given in table IV. After a bit of experimentation, it was found that the required degradation factor for this material was 1.23 and this only needed to be applied to the two elements next to the initially degraded element. The likely reason that the required damage zone wasn't as long as predicted in figure 25 is that the damage zone which develops from degrading the strengths of these two elements only includes some of the quadrature points in each element.

The work presented in this chapter is a possible way that the CDM algorithm could be modified to improve its performance for certain situations in which the scale of discrete damage grows too large for it to be considered in a continuum sense, such as shear damage in textile composites. Significant work remains to be done in determining how these modifications could be applied to a three dimensional model, as well as applying them to non-uniform meshes. Additional validation would need

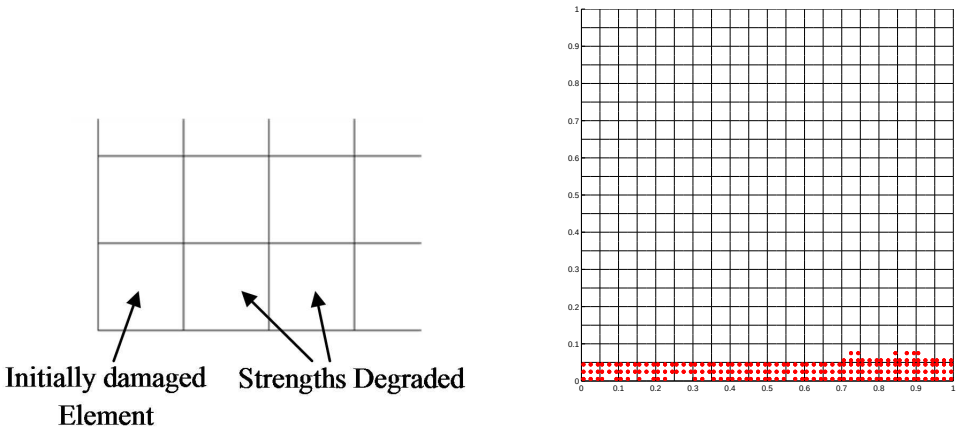

Fig. 29. Strength degradation method and resulting damage zone

to follow, likely including comparison to models in which the damage is discretely modeled as well as experimental results. This validation is particularly important when considering that the success of these modifications is based wholly upon their ability to result in behavior which matches that which is expected and observed in experimentaiton. Such investigations, however, lie beyond the scope of this thesis.

CHAPTER VII

CONCLUSION

The experiments which were conducted overall tend to indicate that when continuum damage mechanics is used to predict damage zone growth in composites resulting from shear failure, it often fails to predict the correct direction of growth. Gorbatikh et al. [1] attributed this poor behavior to the fact that the discrete damage in such models exists on a scale that CDM was not intended to handle, a conclusion which in light of the current research performed appears valid.

It appears that the material anisotropy which exits in composite materials tends to drive the damage zone to grow in a manner contrary to the behavior expected for simple configurations under shear. However, it should be noted that generally, models which experience shear stress concentrations which result from some defect, (i.e. a crack or hole) under global tensile load tend to show logical damage zone growth, provided that the model's mesh is sufficiently refined. Also, it was found that if the stress state around a physical crack under shear is represented with sufficient accuracy, CDM properly predicts a damage zone growing away from the crack tip along the fiber direction. However, for cases where the initial defect (be it a degraded inclusion or a hole) is smooth, is under global shear loading, and is meshed with sufficient refinement, it was found that the CDM approach will always predict damage zone growth across the fibers, contrary to the expected behavior. The overall direction of damage zone growth in such configurations with high eccentricity appears to be closely tied to the location of damage initiation near the tip of the elliptical defect. For these high-eccentricity defects, lower mesh refinement slightly alters the stress distribution near the tip of the ellipse and completely changes the damage zone propagation behavior, causing damage growth along the fibers.

The effect of material anisotropy becomes very apparent in investigations involving uniform meshes with a few degraded elements. It was found that sufficient directional bias in the initially degraded region will result in subsequent damage zone growth that matches the expected behavior. As anisotropy is decreased for these models, the amount of directional bias which is required for obtaining well-behaved damage zone growth decreases to the point that an initially degraded region with no directional bias yields accurate results. This finding suggests that the property degradation scheme tends to drive damage growth in the correct direction, but is unable to overcome the influence of anisotropy for highly orthotropic materials such as carbon-fiber composites.

These findings suggest that it may be possible to modify the basic CDM algorithm to obtain better predictions of damage zone growth for failure modes which do not necessarily match the zone of distributed micro-defects which CDM was originally concieved to model. When damage first occurs, by degrading the strength of the material within a certain geometry around the initial damage, it may be possible to cause a damage zone to form which will result in further damage growth that is consistent with the along-the-fiber matrix cracking which has been observed for composites failing under shear failure.

REFERENCES

[1] L. Gorbatikh, D. Ivanov, S. Lomov, and I. Verpoest, "On modelling of damage evolution in textile composites on meso-level via property degradation approach," *Composites Part A*, vol. 38, no. 12, pp. 2433–2442, 2007.

[2] S. Murakami and N. Ohno, "A continuum theory of creep and creep damage," in *Proc. of 3rd IUTAM Symp. Creep in Structures*, Leicester, England, 1981, pp. 422–444.

[3] S. Murakami, "Mechanical modeling of material damage," *Journal of Applied Mechanics*, vol. 55, no. 2, pp. 280–286, 1988.

[4] J. D. Eshelby, "The determination of the elastic field of an ellipsoidal inclusion, and related problems," *Proceedings of the Royal Society*, vol. 241 A, pp. 376–396, 1957.

[5] L. M. Kachanov., "Rupture time under creep conditions," *Izvestia Akademii Nauk SSSR*, , no. 8, pp. 26–31, 1958.

[6] R. Talreja, "A continuum mechanics characterization of damage in composite materials," *Proceedings of the Royal Society of London, Series A(Mathematical and Physical Sciences)*, vol. 399, no. 1817, pp. 195–216, 1985.

[7] D. M. Blackketter, D. E. Walrath, and A. C. Hansen, "Modeling damage in a plain weave fabirc-reinforced composite material," *Journal of Composites Technology and Research*, vol. 15, no. 2, pp. 136–142, 1993.

[8] C. D. Chapman and J. D. Whitcomb, "Thermally induced damage initiation and growth in plain and satin weave carbon-carbon composites," *Mechanics of composite Materials and Structures*, vol. 7, no. 2, pp. 177–194, 2000.

[9] M. Zako, N Takano, and T. Tsumura, "Numerical prediction of strength of notched UD laminates by analyzing the propagation of intra- and inter-laminar damage," *Materials Science Research International*, vol. 2, no. 2, pp. 117–122, 1996.

[10] M. Zako, Y. Uetsujib, and T. Kurashikia, "Finite element analysis of damaged woven fabric composite materials," *Composites Science and Technology*, vol. 63, no. 3, pp. 507–516, 2003.

[11] J. Choiy and K. K. Tamma, "Woven fabric composite part I: Predictions of homogenized elastic properties and micromechanical damage analysis," *International Journal of Numerical Methods in Engineering*, vol. 50, no. 10, pp. 2285–2298, 2001.

[12] N. Guagliano and E. Riva, "Mechanical behaviour prediction in plain weave composites," *Journal of Strain Analysis*, vol. 36, no. 2, pp. 153–162, 2001.

[13] V. Papaspyropoulos, J. Ahmad, and M. F. Kanninen, "A micromechanical fracture mechanics analysis of a fiber composite laminate containing a defect," in *Effects of Defects in Composite Materials, ASTM STP 836*, pp. 237–249. ASTM, 1984.

VITA

Wesley Ross McLendon was born in Nashville, Tennessee, on August 31, 1983, and moved to Dallas, Texas, shortly thereafter. He began undergraduate studies at Texas A&M University in College Station in August of 2002, studying aerospace engineering and graduating Magna Cum Laude with a Bachelor of Science degree in May of 2007. He began his Master's studies in aerospace engineering at Texas A&M in August of 2007. He plans to pursue a Ph.D. at Texas A&M, preforming research in the area of computational modeling of composite materials.

Department Address:

Texas A&M University

Department of Aerospace Engineering

H.R. Bright Building, Rm. 701, Ross Street - TAMU 3141

College Station TX, 77843-3141

Phone: (214) 893-0286

Email: rossmclendon@tamu.edu rossmclendon@gmail.com